Robust Edge Detection Applied to Multi-Parametric Magnetic Resonance Images

By

Serkalem Damenu Beyene

A Thesis Submitted to the Center of Biomedical Engineering Presented in Partial Fulfillment of the Requirements for the Degree of Master of Science in Biomedical Engineering

Center of Biomedical Engineering

Addis Ababa Institute of Technology

Addis Ababa University

Advisor: Dawit Assefa Haile (PhD)

Addis Ababa, Ethiopia, November 2016

Declaration

I, the undersigned, declare that this MSc thesis is my original work, has not been presented for fulfillment of a degree in this or any other university, and all sources and materials used for the thesis have been acknowledged.

Name: _____

Signature: _____

Date: _____

This MSc. thesis has been submitted for examination with my approval as an advisor.

_____

Dawit Assefa Haile (PhD)

Addis Ababa University

School of Graduate Studies

Certificate of Examination

This is to certify that the thesis prepared by Serkalem Damenu Beyene entitled: *Robust Edge Detection Applied to Multi-Parametric Magnetic Resonance Images* submitted in partial fulfillment of the requirements for the degree of Master of Science in Biomedical Engineering (Imaging and Instrumentation stream) complies with the regulations of the university and meets the accepted standards with respect to originality and quality.

Signed by the Examining Committee:

Examiner _____Signature _____ Date _____

Examiner _____Signature _____Date _____

Examiner _____Signature _____Date _____

Advisor _____Signature _____Date _____

_____

Chief of Department or Graduate program coordinator

Abstract

Robust Edge Detection Applied to Multi-Parametric Magnetic Resonance Images

Various edge detection techniques for color images that have been proposed in the last two decades showed that color images contain 10% additional edge information as compared to their gray scale counterparts. Edge detection is one of the most commonly used operations in medical color image processing. Efficient and accurate edge detection leads to increased performance of subsequent image processing techniques, including image segmentation, object-based image coding, and image retrieval. A color image edge detection algorithm is proposed in this paper that introduces a robust and automated scheme that makes use of higher order statistical features derived from locally computed trinion Fourier transforms. The proposed scheme uses a holistic vectorial representation of the color images in the three (trinion) space and applies trinion based Fourier transforms to extract useful imaging features for the purpose of edge detection of multi parametric magnetic resonance images (MP-MRI). A suitable color space transformation and a way of extracting robust higher order features are included in the method. Performance of the proposed scheme is compared against classical edge detection methods and other vectorial approaches which have been proposed in the literature. Results have shown that none of the classical as well as the other vectorial approaches were able to detect useful edges. Application of the method is shown in edge detection on MP-MR images of brain scans of patients treated for Glioblastoma multiforme (GBM). The algorithm performs well in detecting the tumor edges, that was (qualitatively) in a very good agreement with the ground truth information which is the oncologist's contour drawn manually.

Key Words: Color Image processing, Edge detection, Trinion, Quaternion, Magnetic Resonance Image.

Acknowledgment

Here is my deepest gratitude to my advisor Dr. Dawit Assefa Haile (PhD) for his uninterrupted encouragement, guidance and supervision throughout this thesis work. The discussions held with him helped me to organize the material well and to grow up my knowledge in different aspects of medical image processing. I am grateful to his motivation for the timely completion of the research, and his dynamic suggestions for solutions to any challenges during the total work of this thesis.

I am also thankful to Ayder Referral Hospital-Mekelle University, Pioneers Diagnosis Center and Yehuleshet Higher Clinic for providing me the testing data sets.

My special thanks also goes to Dr. Mihla Zebenigus (Neurologist) at Yehulishet higher clinic who facilitated things for me to learn the whole process during image acquisition in their MRI department, and also providing her expertise in interpreting the preliminary results in the thesis work.

Finally to those who encouraged me and showed me great affection throughout this thesis work, my sincere thank is here, Thank you all.

Table of Contents

List of Figures

List of Tables

Acronyms

ACR-NEMA	American College of Radiology and the National Electrical Manufacturers Association
ADC	Analog-to-Digital Converter
AET	Application Entity Title
AV	Arteriovenous
CCD	Charge-Coupled Device
CMYK	Cyan - Magenta -Yellow and Black
CRT	Cathode Ray Tube
CSF	Cerebrospinal Fluid
CT	Computed Tomography
DR	Difference Vector
FLAIR	Fluid Attenuated Inversion Recovery
FMFE	Fast Multilevel Fuzzy Enhancement
GAP	Gradient Adjusted Predictor
GBM	Glioblastoma Multiforme
HSI	Hue- Saturation- Intensity
HSL	Hue- Saturation- Luminance
HSV	Hue- Saturation- Value
MP-MRI	Multi-Parametric Magnetic Resonance Image
NMS	Non Maximum Suppression
NMR	Nuclear Magnetic Resonance
NRI	Nuclear Resonance Image

PET	Positron Emission Tomography
RF	Radio Frequency
RGB	Red- Green- Blue
SNR	Signal- to- Noise Ratio
SPECT	Single Photon Emission Computerized Tomography
TFT	Trinion Fourier Transform
WT	Wavelet Transform

1. Introduction

1.1. Background

The subject of color image processing has gained increasing recent attention because color images convey more information about objects in a scene than gray-scale images and this information can be used to further refine the performance of an imaging system. One of the fundamental tasks in image processing is edge detection. The performance of high level image processing such as object recognition, segmentation, image coding, and robot vision, depends on the accuracy of edge detection since edges contain essential image information. An effective edge detector reduces a large amount of data but still keeps most of the important features of the image.

Human visual perception doesn't differentiate color separately (into its components) but tends to process it as a whole (as one entity). In this sense, the compact representation of colors as vectors and operating on these vectors are particularly interesting. This gave rise to the development of algorithms in useful but challenging applications such as nonlinear vector filters. The available edge detection techniques do not treat the color images wholly, but consider the different color components/bands/channels as separate monochrome images. This is primarily because there is no simple mathematical framework for the linear filters to be applied on color images. The main drawback of such methods is that color component separation misses out the information as to how the different color bands are correlated to each other while it is now well proved that when the correlation among the color bands are exploited the respective image processing algorithms yield more accurate results [8-10].

Quantitative image processing approaches that make use of such inter correlation information are proved to be efficient in many applications. One such interesting area of research in image processing is color image edge detection. Color edge detection is proved to be superior

to its gray scale counterparts. Various monochromatic as well as the sounder vectorial techniques have been proposed in the literature for use in edge detection [1–5]. Some of these include: Vector Gradients, Classical method, Sobel operator, Robert's cross operator, Prewitt's operator, Laplacian Operator, Canny edge detection algorithm and the like. A good review and detailed comparison of different edge detection schemes can be found in [6]. Generally, in various applications, the vectorial approaches are shown to be more efficient in edge detection of color images compared to most serial schemes. This is mainly because the vectorial methods can manipulate the inter correlation between color channels that make up the color image. This advantage of the vectorial schemes is also accompanied by a substantial saving of computation time and data storage to be achieved. In this regard, a core issue is then finding an efficient color representation scheme.

Integral transforms such as the Gabor transform and wavelets are known to be major pillars in edge detections. Using such transformations help to represent each component of a given color image in the real (or complex) space separately and analyze them serially. In certain applications, such as linear color filtering, where the inter-correlation between color channels is less important, such an approach may be adequate. However, in many other applications, such as color- auto and cross-correlations, nonlinear vector filtering, texture analysis and the like, the inter–correlation among the multiple color channels carries very useful information which limits the applicability of the above mentioned transforms. A work around this issue, however, has been realized through the use of higher dimensional algebras and related hyper-complex Fourier Transforms. One such a holistic approach that showed great promises in color image analysis makes use of the well-known quaternions [7] in four spaces and the recently proposed trinions [8] in three spaces. The novelty of such an approach is that it allows every pixel or voxel of color images to be represented vectorially as one entity or object, keeping the information as to how the multiple color channels are correlated to each

other. The analysis can be carried out holistically using the respective vector valued integral transforms.

Researches have shown a promising way of tissue identification and classification of multi-parametric magnetic resonance images (MP-MRI) of the brain, applied to patients treated for the most common and aggressive of the gliomas known by the name Glioblastoma multiforme (GBM) [9-10]. The study investigates a robust and automatic tool that uniquely and efficiently characterizes/ identifies different tissue structures, specifically on the brain, such as tumors, necrotic tissue, edema, normal tissues and the like, based on MP-MR image processing. In order to carry out the task, the study applies a rigorous mathematical algorithmic analysis. It was a signal analysis based approach that reveals useful signatures for glioma tumors which may have a potential to assist automatic and accurate tumor demarcation (segmentation). Inspired by recent applications of higher dimensional Fourier transforms in color image analysis, the scheme treats MP-MR images as multi band colors represented in a holistic manner in the higher dimensional algebraic spaces. A color edge detection scheme for MP-MR images is proposed in this thesis making use of statistical features derived from a spatially localized analysis in the trinion and quaternion spaces.

1.2. Statement of the Problem

Techniques and methods which are classified as very modern still treat color images as separated monochromatic images for edge detection and processing [6] . But such a method has a potential drawback because by taking the different bands separately we are losing important information about how the different image components making up the general image are correlated to each other. And since each component is considered separately, the computational time and space requirement during analysis will be considerably high.

It is sometimes possible to transform a given multi component color image into single component gray scale and do the edge detection analysis on a new space. There are instances where this method gives satisfactory results for some applications. However, the right solution is to develop a method that incorporates all the color components and the correlations between them which provides a better approach in handling color edges. The second existing challenge that motivates this thesis work is that mostly in our clinics images acquired through different modalities (in our case these are MP-MRI) are interpreted visually for various purposes be it for tumor demarcation, biomarker identification, and the like.

Considering these drawbacks mentioned above, it could be vital to come up with a new and robust method or technique for color edge detection that will be applied on MP-MR images and can avoid representing different sequences of MRI as separate monochromatic images but rather treat them holistically using vectors without the need for the decoupling. In that regard, this thesis intends to develop an accurate, simple, fast, and automated algorithmic scheme mainly for use in tissue edge detection (focusing on cancers) of MP-MR images taken from cohorts of study done on patients treated for the highest grade glioma known by the name Glioblastoma multiforme (GBM) and similar other subjects [10].

1.3. Objectives of the Study

This research work is mainly aimed to come up with automated edge detection technique which is capable of representing the correlations between color components and applied for MP-MR images with the following general and specific objectives.

- **General objective:**

✓ To develop an efficient edge detection algorithm that can represent the different components of MP-MR images of the brain holistically and performs feature extraction

that can be used in robust and automated cancer tissue demarcation with a potential application in patients response (disease progression, survival, etc.) quantification.

- **Specific Objectives:**

✓ The development of a multi-parametric model to combine parameters derived from measurement of multi-modality MR images (T1 and T2 relaxation, diffusion weighted imaging, proton density, and dynamic contrast-enhanced MRI) to improve the discrimination between normal and malignant peripheral zone tissues through edge detection.

✓ Review different techniques of edge detection which are available on the literature.

✓ Develop an algorithm that reduces the information loss during edge detection.

✓ Implement the algorithm on MP-MR images.

1.4. Applicability of the Study

The growing incidence of brain tumors increases the number of images that need to be reviewed by physicians. In addition, the high cost of examinations and the lack of specialists prevent many patients from receiving effective treatment. So this automated edge detection of brain tumors can serve as a tool to segment or classify the tumor type and localize the exact location and offers many potential benefits. In a screening setting, it allows the examination of a large number of images in less time and more objectively than current observer driven techniques. In a clinical setting, it can be an important diagnostic aid and can reduce the workload of trained graders, and, thereby reducing costs. In addition, the work could have real potential applications in patients' response quantification following therapies. Moreover, the edge detection method that will be proposed can be applied in other medical and non-medical fields where clear color edges of materials is needed for different tasks like in designs, forensics, and the like.

1.5. Scope and Limitation of the Study

The research will be conducted to develop a color edge detection algorithm and will be applied on MP-MR images of the brain data taken from a cohort. The data comes with expert ground truth information which has been used in the current research as a gold standard. Note that all the results presented in this thesis might require extensive validation work comprising of an observer study.

1.6. Organization of the thesis

Chapter one is introductory part giving a background of the study. The basic problem is described there. The objectives of the thesis work, applicability of the thesis followed by scope and limitation of the study are also described. Chapter two presents literature review on different edge detection methods. Chapter three introduces imaging, MP-MR images and about brain tumors. Chapter four deals with color medical image processing while chapter five presents the proposed trinion based edge detection scheme. Results and discussions are presented in chapter six. Finally chapter seven presents conclusions, recommendations and future directions.

2. Edges and Edge Detection Methods

The digital image processing community has developed several image processing techniques such as different edge detection schemes which many of them are ad hoc [11]. Accordingly, most of the available litrature has divided the edge detection methods into two catagories: gray/monochromatic and color [11]. Even if the main concern of this thesis work is on development of holistic vectorial color edge detection, it is important to discuss first some basic definitions and concepts about edges and edge detection schemes developed by different scholars, related litatures including conceptual issues regarding classical methods of gray scale edge detection,different monochromatic color edge detection methods, and finally vectorial color edge detection techniques which are intial bases for this thesis work.

2.1. Definition of Edges

Many scholars define edges in different context. Edges are pixels where image brightness changes abruptly (for gray scale images, for example). Edge is neighboring pixels with large differences in value. Edge is also a part of an image that contains significant variation [11]. In an image we can find edges between two different regions. The important visual information that is extracted from edge of an image is because of variations in physical, photometrical or geometrical properties in the scene. Physical variations include variations in the reflectance, illumination, orientation, and depth of scene surfaces. Since image intensity is often proportional to scene radiance, physical edges are represented by changes in the intensity function of an image.

2.1.1. Types of Edges

The most known edge types include: step edge, line edge and junction edge.

1. Step edge: it generally occurs between two regions having almost constant, but different, grey levels. The step edges are the points at which the grey level discontinuity occurs, and

localized at the inflection points. Moreover, localization of step edges can be either as positive maxima or negative minima of the first-order derivative or as zero-crossings of the second-order derivative as shown in Fig.(2.1) [11]. One model example of step edge is double step edge. Again this double step edge type can be classified into pulse and staircase as shown in Fig. (2.2). Ramp edge is a step edge where the intensity change is not instantaneous but occurs over a finite distance.

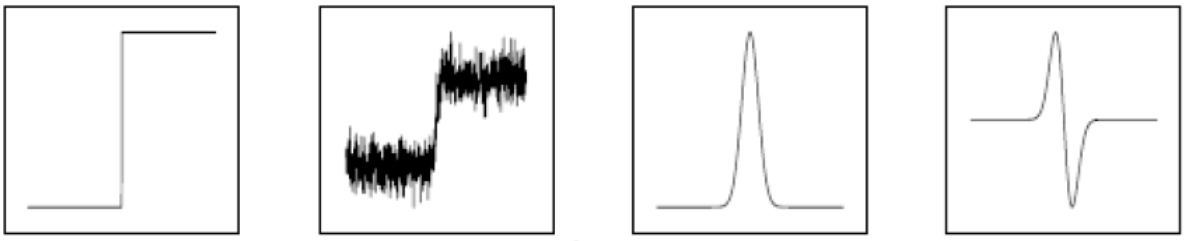

(a) (b) (c) (d)

Figure 2.1: a) ideal step edge, b) smoothed step edge corrupted by noise, c) first-order derivative, d) second- order derivative of the smoothed step edge corrupted by noise (left-right).

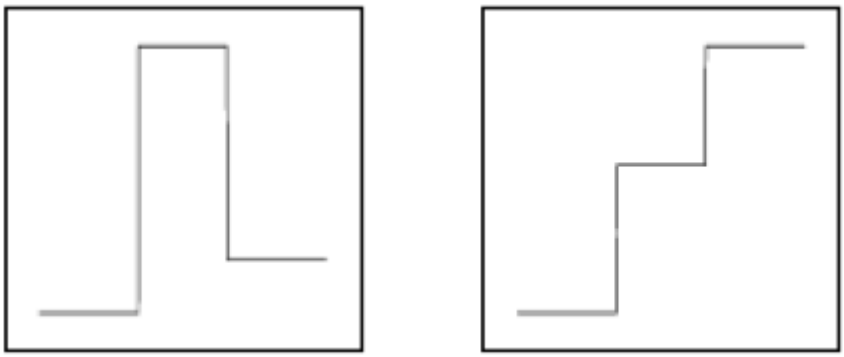

Figure 2.2: Profile of pulse (left) and staircase (right) step edges.

2. Line edge: the image intensity abruptly changes value but then returns to the starting value within some short distance (generated usually by lines). Such edges are localized as zero crossings of the first derivative, or local maxima of the Laplacian, or local maxima of the grey level variance of the smoothed image. This type of edge is successfully used in remote

sensing images for instance to detect roads and rivers [11]. Figure 2.3 (left) illustrates a line edge.

3. Junction edge: this type of edge is formed when two or more edges meet together. They are created or produced mainly by illumination or occlusion effect. The junction can be localized in various ways: e.g., a point with high curvature, or a point with great variation in gradient direction, or a zero-crossing of the Laplacian with high curvature or near an elliptic extremum [11] as illustrated on Fig. 2.3 (right).

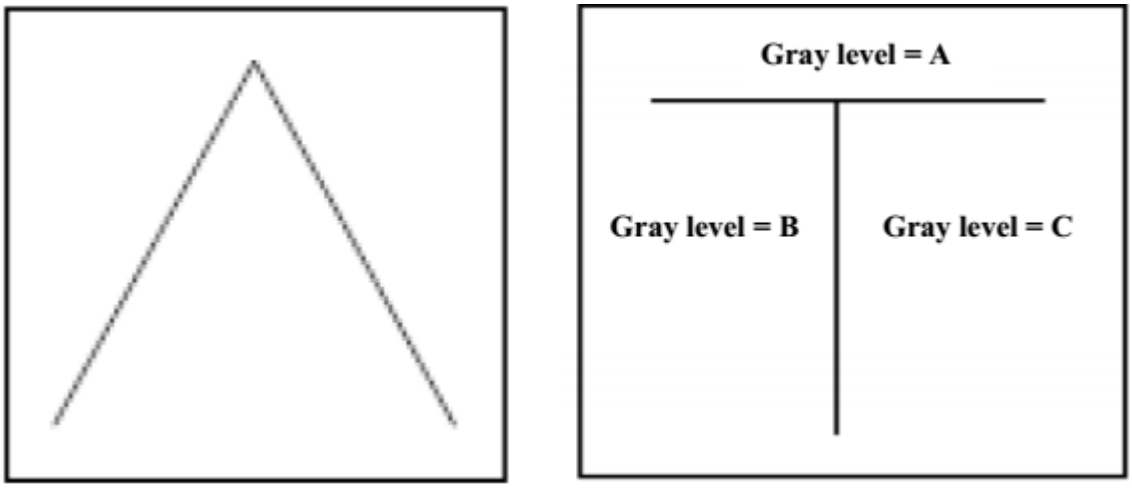

Figure 2.3: Profile of line edges and junction edges from left to right.

2.1.2. Steps of Edge Detection

Most algorithms for edge detection involve four main steps that can be discussed as follows.

i. **Filtering or smoothing**: the first step to go through edge detection is filtering. By this image processing the performance of an edge detector with respect to noise can be improved. However, there is a trade-off between edge strength and noise reduction. Applying more filtering to reduce noise often results in a loss of edge strength.

ii. **Enhancement**: this step facilitates the detection of edges. Enhancement emphasizes pixels where there is a significant change in local intensity values and is usually performed by computing the gradient magnitude.

iii. **Detection**: determines which edge pixels should be discarded as noise and which should be retained. We only want points with strong edge content. However, many points in an image have a nonzero value for the gradient, and not all of these points are edges for a particular application. Therefore, some method should be used to determine which points are edge points. Usually, thresholding provides the criterion used for detection.

iv. **Localization**: determines the exact location of an edge. Edge thinning and linking are usually required in this step.

2.2. Edge Detectors

An edge detector can be defined as an algorithm that produces sets of edges from an image. An edge detector can be defined also as an algorithm that accepts a digital image as input and produces an edge map as output [11]. For gray level edge detection the edge detector can be classified in two broad categories [13] as described below (see Fig. 2.4).

2.2.1. First Order Edge Detection/Gradient Based Edge Operators

It is generally known that calculus explains continuous functions using derivatives. An image is a two dimensional functional (function of functions) in which operators describing edges can be expressed by partial derivatives. Points which lie on an edge can be detected by detecting local maxima or minima of the first derivative. If $I(x, y)$ is the input image, then the image gradient is given by the following formula:

$$\nabla I(x,y) = \left(\frac{\partial I(x,y)}{\partial x}, \frac{\partial I(x,y)}{\partial y} \right) = \left(G_x, G_y \right) \tag{2.1}$$

where $\frac{\partial I(x,y)}{\partial x}$ is the gradient in the x direction, $\frac{\partial I(x,y)}{\partial y}$ is the gradient in the y direction.

The gradient magnitude and direction can be computed by the following formulas:

$$|G| = \sqrt{\left(\frac{\partial I}{\partial x}\right)^2 + \left(\frac{\partial I}{\partial y}\right)^2} \tag{2.2}$$

$$\theta = \arctan\left(G_y / G_x\right) \tag{2.3}$$

From the equations, the magnitude of the gradient computed gives edge strength and the gradient direction is always perpendicular to the direction of the edge.

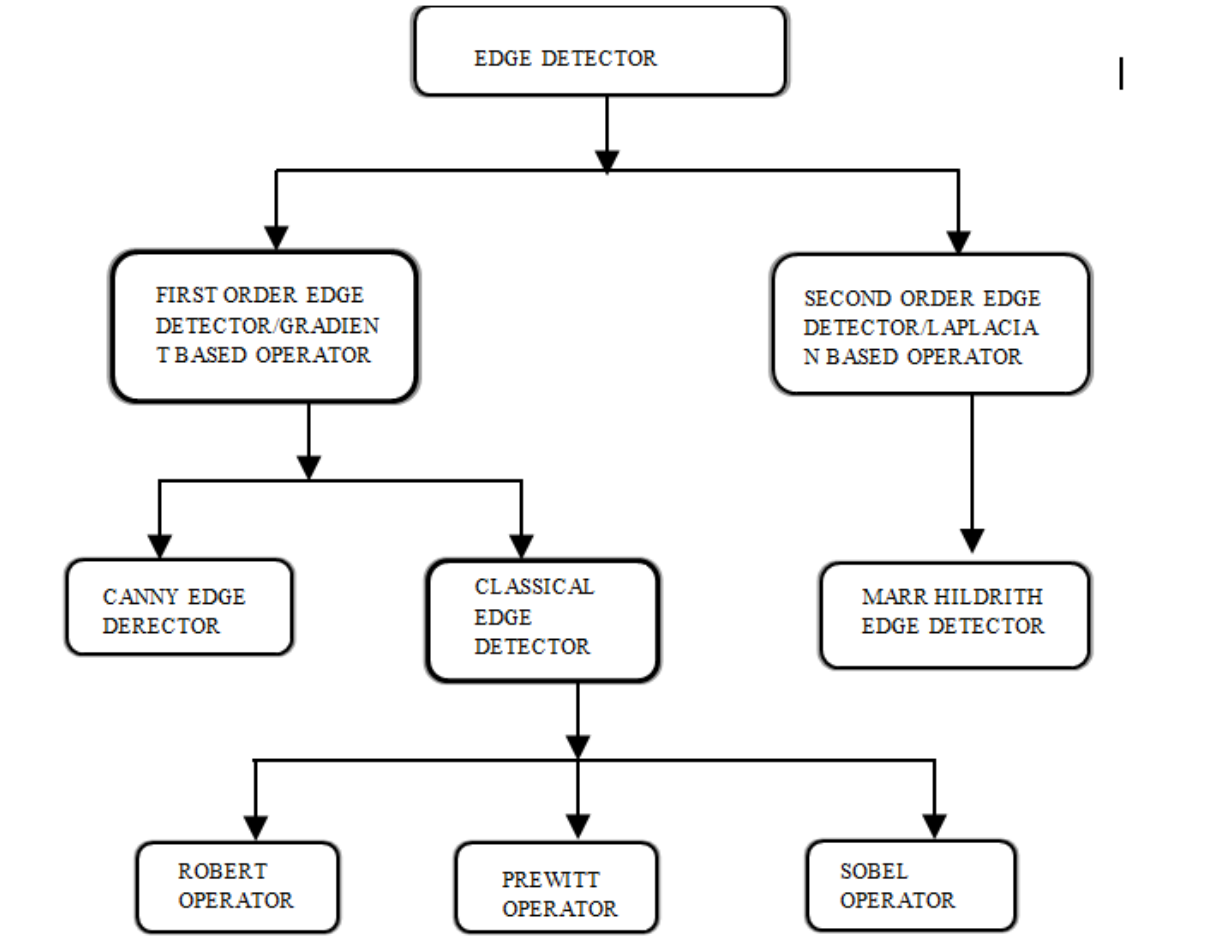

Figure 2.4: Types of edge detectors in gray level edge detection.

2.2.1.1. Classical Edge Detectors

As shown in Fig. (2.4), classical edge detectors includes: Robert, Sobel, and Prewitt operators which are easy to operate but highly sensitive to noise and those are discussed below. Figure (2.5) presents flow chart of general algorithm for classical edge detectors [13].

Roberts Edge Detector

The Roberts edge detection technique is the most basic of all the techniques of classical edge detectors. It performs a simple, quick to compute, gradient measurement on an image. Pixel values at each point in the output represent the estimated absolute magnitude of the spatial gradient of the input image at that point. The operator consists of a pair of 2×2 convolution kernels as shown in Eqn. (2.4). Extension to the higher image dimensions is not possible in this edge detection technique [14]. Roberts operator uses the following kernels, D_x and D_y, in the respective directions.

$$D_x = \begin{bmatrix} 0 & -1 \\ 1 & 0 \end{bmatrix} \text{ and } D_y = \begin{bmatrix} -1 & 0 \\ 0 & 1 \end{bmatrix} \tag{2.4}$$

Sobel Edge Detector

Sobel operator is a discrete differentiation operator used to compute an approximation of the gradient of image intensity function for edge detection. At each pixel of an image, Sobel operator gives either the corresponding gradient vector or normal to the vector. It convolves the input image with a kernel and computes the gradient magnitude and direction. It uses the following 3x3 two kernels [14].

$$D_x = \begin{bmatrix} -1 & 0 & 1 \\ -2 & 0 & 2 \\ -1 & 0 & 1 \end{bmatrix} \text{ and } D_y = \begin{bmatrix} -1 & -2 & -1 \\ 0 & 0 & 0 \\ 1 & 2 & 1 \end{bmatrix} \tag{2.5}$$

As compared to Roberts's operator, Sobel has slow computation ability but has large kernel so it is less sensitive to noise. As having larger mask, errors due to effects of noise are reduced by local averaging within the neighborhood of the mask.

Prewitt Edge Detector

The Prewitt is another operator used for edge detection. This operator does not place any pixels which are closer to the center of the mask. Technically, it is a discrete differentiation operator, computing the gradient of an image intensity function. At each pixel in the image, the result of the Prewitt operator shows the corresponding gradient vector or the norm of this vector. The Prewitt operator is based on convolving the image with a small, separable, and integer valued filter in horizontal and vertical directions and is therefore relatively inexpensive in terms of computations. On the other hand, the gradient operator is relatively crude for high frequency variations in the image. Prewitt operator is similar to the Sobel operator and is used for detecting vertical and horizontal edges in images. In simple terms, the operator calculates the gradient vector of the image intensity at each point, giving the direction of the largest possible increase from light to dark and the rate of change in that direction. The function of Prewitt edge detector is almost same as of Sobel detector but have different kernels [13, 14].

$$D_x = \begin{bmatrix} -1 & 0 & 1 \\ -1 & 0 & 1 \\ -1 & 0 & 1 \end{bmatrix} \text{and } D_y = \begin{bmatrix} -1 & -1 & -1 \\ 0 & 0 & 0 \\ 1 & 1 & 1 \end{bmatrix} \tag{2.6}$$

Many researches proved that Prewitt edge detector has better performance than that of Sobel operator [13].

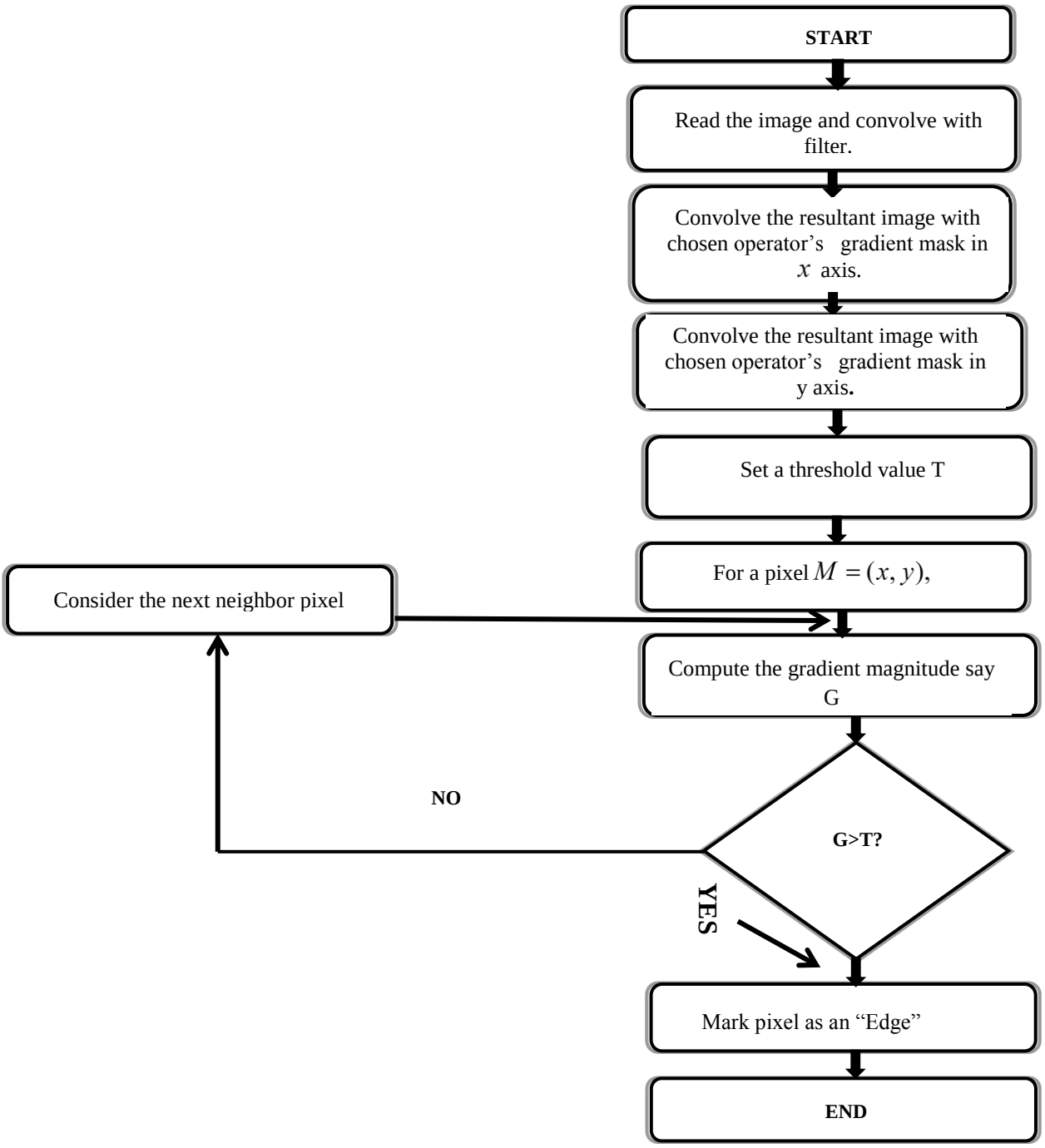

Figure 2.5: Flow chart of general algorithm for classical edge detectors [13].

2.2.1.2. Canny Edge Detector

The Canny edge detection operator was developed by John F. Canny in 1986 and uses a multi-stage algorithm to detect a wide range of edges in images. An optimal edge detector is based on the following three criteria [14]: good detection (the algorithm should mark as many real edges in the image as possible), good localization (marked edges should be as close as

possible to the edge in the real scene), and minimal response (a given edge in the image should only be marked once, and where possible, image noises should not create false edges). Based on these criteria, the canny edge detection process includes the following stages:

Step I (Noise reduction by smoothing): Using the Gaussian filter, noise contained in the image is smoothed by convolving the input image $I=(x,y)$ with the filter. Then, the smooth resultant image is computed through convolution as:

$$f(x,y)=g(x,y)*I(x,y) \tag{2.7}$$

Step II (Finding gradients): in this step the edge is detected where the change in gray scale intensity is maximum. Required areas are determined with the help of gradient of images. Sobel operator is used to determine the gradient at each pixel of the smoothened image. The Sobel operators in x and y directions are given as:

$$D_x=\begin{bmatrix}-1 & 0 & 1\\ -2 & 0 & 2\\ -1 & 0 & 1\end{bmatrix} \text{and } D_y=\begin{bmatrix}1 & 2 & 1\\ 0 & 0 & 0\\ -1 & -2 & -1\end{bmatrix} \tag{2.8}$$

Then, the above Sobel masks are convolved with the smoothed image to give gradients in x and y directions.

$$G_x=D_x*f(x,y) \text{ and } G_y=D_y*f(x,y) \tag{2.9}$$

From Eqn. (2.9) it is possible to drive a formula for edge strength or magnitude of gradient of a pixel and the direction of the gradient as follows:

$$|G|=\sqrt{G_x{}^2+G_y{}^2} \tag{2.10}$$

$$\theta = \arctan\left(\frac{G_y}{G_x}\right) \tag{2.11}$$

Step III (Non maximum suppressions): The algorithm tracks along these already highlighted regions and suppresses any pixel that is not at the maximum.

Step IV (Hysteresis thresholding): This is the last step that Canny edge detector follows. In this step the output of non-maxima suppression still contains the local maxima created by noise. Instead of choosing a single threshold, for avoiding the problem of streaking two thresholds t_{high} and t_{low} are used. For a pixel $M(x, y)$ having gradient magnitude $|G|$ following conditions apply to detect pixel as edge: If $|G| < t_{low}$ then discard the edge and if $|G| > t_{high}$ keep the edge. If $t_{low} < |G| < t_{high}$ and any of its neighbors in a 3 ×3 region around it have gradient magnitudes greater than $t_{high,}$ keep the edge. If none of pixel (x, y)'s neighbors have high gradient magnitudes but at least one falls between t_{low} and t_{high} search the 5 × 5 region to see if any of these pixels have a magnitude greater than t_{high}. If so, keep the edge. Else, discard the edge. Figure (2.6) illustrates flow chart of the Canny edge detection algorithm [13].

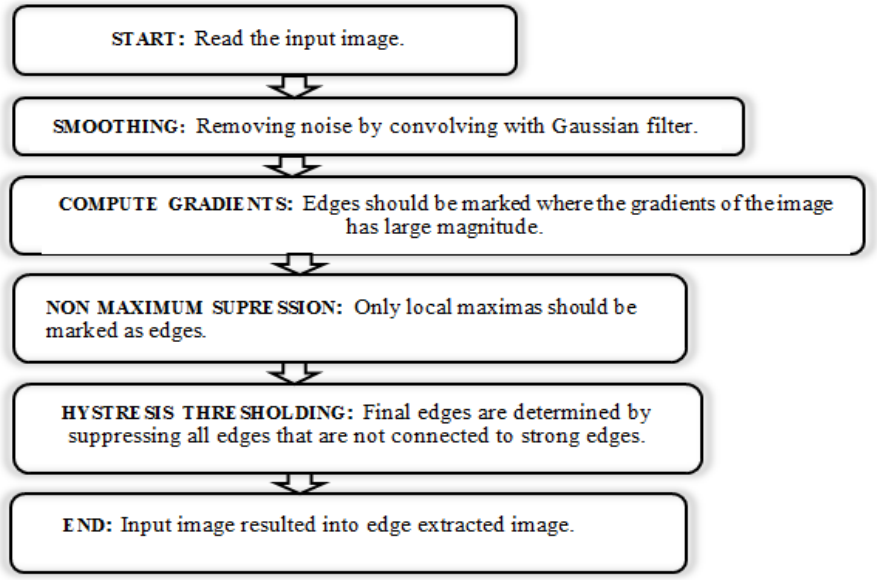

Figure 2.6: Flow chart of Canny edge detection algorithm.

2.2.2. Second Order Edge Detectors

It is based on second order derivatives. In this operator a pixel is marked as an edge at a position where second derivative of an image becomes zero. The Laplacian is often used in such kinds of edge operators. The Laplacian ∇^2 of a 2D image $I(x, y)$ is defined as follows [16]:

$$\nabla^2 I(x,y) = \frac{\partial^2}{\partial x^2} I(x,y) + \frac{\partial^2}{\partial y^2} I(x,y) \tag{2.12}$$

2.2.2.1. Laplacian of Gaussian or Marr Hildreth Operator

This second order edge detector uses the Laplacian to take the second derivative of an image. It works based on zero crossing approach. It uses both Gaussian and Laplacian operator so that Gaussian operator reduces the noise and the Laplacian operator detects the sharp edges. The Gaussian operator is given by [16]:

$$G(x,y) = \frac{1}{\sqrt{2\pi\delta^2}} \exp^{-\left(\frac{x^2+y^2}{2\delta^2}\right)} \tag{2.13}$$

where δ is the standard deviation (Gaussian width).

Then the Laplacian of the Gaussian (LOG) operator can be computed as follows:

$$\text{LOG} = \frac{\partial^2}{\partial x^2} G(x,y) + \frac{\partial^2}{\partial y^2} G(x,y) = \frac{x^2 + y^2 - 2\delta^2}{\delta^4} \exp^{-\left(\frac{x^2+y^2}{2\delta^2}\right)} \tag{2.14}$$

Limitations of the Marr-Hildreth Operator: these include the fact that it gives responses that do not correspond to edges, so called "false edge". Also it is prone to localization error at curved edges.

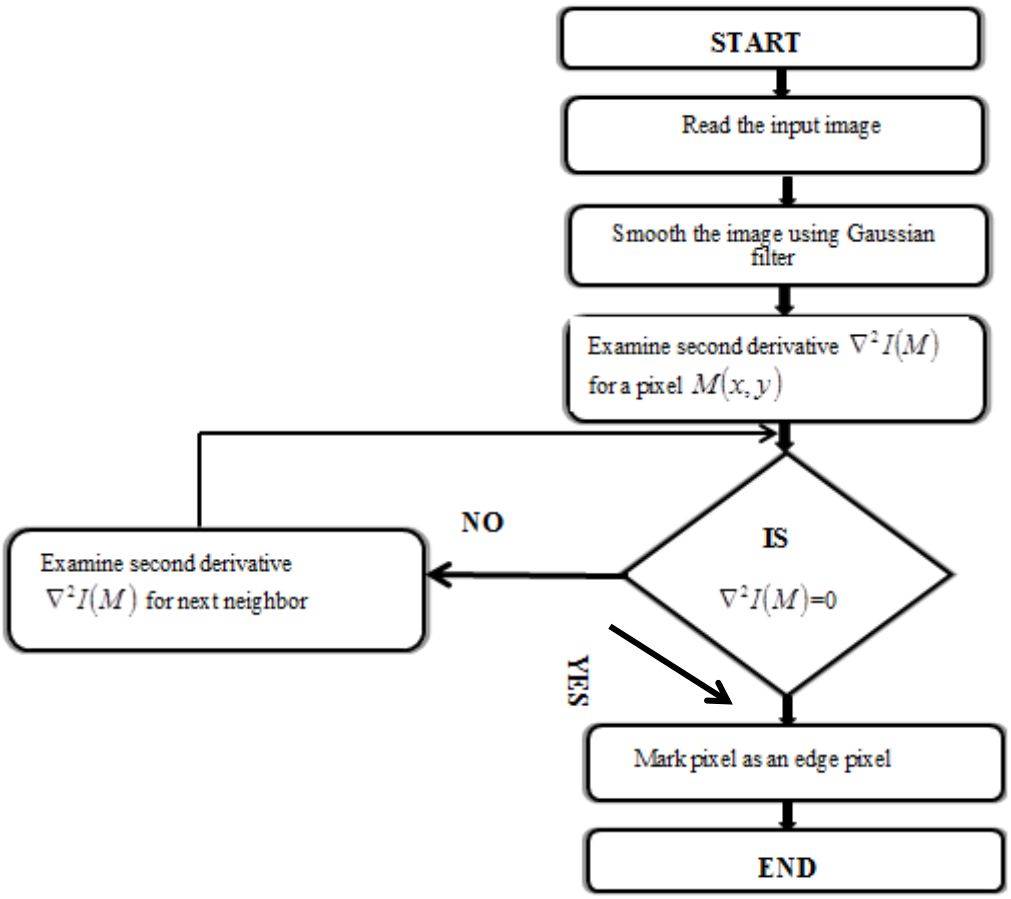

Figure 2.7: Flow chart of general algorithm for Laplacian of Gaussian operator [13].

Comparing the different edge detectors

Comparing the above edge detection operators, it is found that canny gives a better optimum edge detection results. The followings are some points that made canny edge detector better.

Less sensitive to noise: As compared to operators like Prewitt, Robert and Sobel canny edge detector is less sensitive to noise. It uses Gaussian filter which removes noise at a great extent as compared to other filters. LoG operator is also highly sensitive to noise in comparison to canny operator.

Remove streaking problem: Operators like Robert use single thresholding technique but it results into streaking. Streaking means, if the edge gradient just above and just below the set threshold limit it removes the useful part of connected edge, and leave the disconnected final

edge. To circumvent this drawback, canny detector uses 'hysteresis' technique which uses two threshold values t_{low} and t_{high} as discussed above in the canny algorithm.

Adaptive in nature: Classical operators have fixed kernels so cannot be adapted to a given image. While the performance of Canny algorithm depends on variables or adjustable parameters like σ, which is the standard deviation of Gaussian filter, and threshold values t_{low} and $t_{high.}$ Smaller value of σ results in smaller Gaussian filters which in turn results in finer edges. So users can change these parameters and can improve the results of the canny algorithm.

Good localization: LoG operators cannot find edge orientation while canny operator provides edge gradient orientation which results into good localization.

2.3. Edge Detection Approaches

This section summarizes dominant approaches in the world of edge detection methods and explains their advantages and drawbacks and the relationships among them. Some works, because of their importance and fundamental impacts, are described in more details, while some have been reviewed with just referring to their main contributions. There are different methods and techniques developed to perform edge detection in image processing. However, the most known ones may be grouped into two categories: Gray/monochromatic and color edge detection.

2.3.1. Gray/Monochromatic Edge Detection Method

There are different edge detection schemes suggested in the literature for use in gray scale edge detection. Some of these include:

Classical Methods: including Sobel (1970), Prewitt (1970), Kirsch (1971), Robinson (1977), and Frei-Chen (1977) [11]. They compute an estimation of gradient for the pixels, and look

for local maxima to localize step edges. Typically, they are simple in computation and capable to detect the edges and their orientation, but due to lack of smoothing stage, they are very sensitive to noise and generally suffer inaccuracies.

Gaussian Based Methods: Marr and Hildreth [25, 26] were the pioneers that proposed an edge detector based on Gaussian filter. Their method had been a very popular one, before Canny released his detector. They originally pointed out the fact that the variation of image intensity (i.e. edge) occurs at different levels. This implied the demand to smoothing filters with different scales, since a single filter cannot be optimal for all possible levels. They suggested the 2D Gaussian function, defined above by Eqn. 2.13 as the smoothing operator.
Multi-Resolution Methods: Multi-resolution methods incorporate repeating edge detection for several scales of the Gaussian filter to achieve a quality performance. The main challenges in these methods includes selection of a proper range for the scales, combination of the outputs corresponding to different scales, and adaptation to level of noise in the image. There are plenty of publications that apply multi-resolution method of edge detection for gray scale edge detection and few are the followings:

In [27], Schunck introduced an algorithm for the detection of step edges using Gaussian filters at multiple scales. The initial steps of Schunck‘s algorithm are based on Canny‘s method. The algorithm begins by convolving an image with a Gaussian function. The gradient magnitude and gradient angle are then computed for each point in the resulting smoothed data array. Next, the gradient ridges in the results of the convolution are thinned using non maxima suppression (NMS). Then, the thinned gradient magnitudes are thresholded to produce the edge map.

Witkin [28] studied the property of zero-crossings across scales for 1D signal. He marked the zero-crossings of second derivative of a signal smoothed by Gaussian function in a range of

scale, and then presented them versus scales. This representation, known as the scale-space representation of a signal, contains the location of a zero-crossing at all scales starting from the smallest scale to the scale at which it disappears. This work initiated the study of edge detection as a function of scale, and led to algorithms that combine edges for better edge detection.

Bergholm [29] proposed an algorithm which uses the Gaussian filter and combines edge information moving from a coarse-to-fine scale. His method is called edge focusing, and uses a rule-based approach for detecting local features and for tracking and predicting a possible scale parameter. Both the Marr-Hildreth and Canny edge-detectors are possible schemes that can be used in edge focusing.

Lacroix [30] avoids the problem of splitting edges by tracking edges from a fine-to-coarse resolution. His algorithm detects edges using the Canny method of non-maxima suppression (NMS) of the magnitude of the gradient in the gradient direction. His method then considers three scales: σ0, σ1, and σ2. The smallest scale, σ0, is the detection scale, and is the finest resolution at which a group of edges appears. The largest scale, σ2, is the blurring scale, and is the coarsest resolution at which the first appeared edges still remains. The intermediate resolution is computed as:

$$\sigma_1 = \sigma_0 + \frac{\sigma_2 - \sigma_0}{3} \tag{2.15}$$

The first appeared edges are validated as long as they are local maxima in the Gaussian gradient and the two recent regions are homogeneous and significantly different from one another. Only validated edges are then tracked through the scales. Although Lacroix avoids the problem of splitting edges, he introduces the problem of localization error as it is the

coarsest resolution that is used to determine the location of the edges. He also provides no explanation as to how to decide which scales are to be used and under what conditions.

Williams and Shah [31] devised a scheme to find edge contours using multiple scales. They analyzed the movement of edge points smoothed with a Gaussian operator of different sizes, and used this information to determine how to link edge points detected at different scales. Their method, following the lead of Canny, uses a gradient of Gaussian operator to determine gradient magnitude and direction, followed by non-maxima suppression (NMS) to identify ridges in the gradient map.

Deng and Cahill [32] also used an adaptive Gaussian filtering algorithm for edge detection. Their method is based on adapting the variance of the Gaussian filter to the noise characteristics and the local variance of the image data. Based on observations of how the human eye perceives edges in different images, they concluded that in areas with sharp edges, the filter variance should be small to preserve the sharp edges and keep the distortion small. In smooth areas, the variance should be large so as to filter out noise.

In [33], Bennamoun et al. presented a hybrid detector that divides the tasks of edge localization and noise suppression between two sub detectors. This detector is the combination of the outputs from the Gradient of Gaussian and Laplacian of Gaussian detectors. The hybrid detector performs better than both the first-order and second-order detectors alone, in terms of localization and noise removal. The authors extended the work to automatically determine the optimal scale and threshold of the hybrid detector. They do this by deriving a cost function which maximizes the probability of detecting an edge for a signal with noise and simultaneously minimizes the probability of detecting an edge in noise only [19].

Nonlinear Methods: Perona and Malik [34] proposed a scale space representation of an image based on anisotropic diffusion. The essential idea here is to allow space variant blurring. The goal is to smooth within a region and keep the boundaries sharp. A high value for the diffusion constant within the region and a very small value (possibly 0) on the boundary can produce the desired effect. This effectively leads to a spatially adaptive smoothing which tends to preserve the location of edges throughout the scale hierarchy.

Wavelet transform (WT) Methods: the (discrete) wavelet transform is defined as the sum over the entire of rows and columns (i.e. spatial domain) of the image intensity function multiplied by scaled and shifted versions of the mother wavelet function. It results in coefficients that are function of the scale and shifts. In other word, WT maps the image into a space with two variables: scale and shift. The scale represents the function by compressing or stretching it, and denotes its features in frequency domain, while the shift corresponds to the translation of the wavelet function in the spatial domain (i.e. row or column). There is a correspondence between scale and frequency: a low scale shows the rapidly changing details of the intensity function with a high frequency, and a high scale illustrates slowly changing coarse features with a low frequency. Therefore, WT acts as a mathematical microscope, in which one can monitor different parts of an image by just adjusting focus on scale. An important property of WT is its ability to focus on localized structures, e.g. edges, with a zooming procedure that progressively reduces the scale parameter. In this way, coarse and fine signal structures are simultaneously analyzed at different scales.

Heric and Zazula [20] presented an edge detection algorithm using the Haar wavelet transform. They chose Haar wavelet as the mother wavelet function, because it was orthogonal, compact and without spatial shifting in the transform space. By applying WT, they presented the intensity magnitude variation between adjacent intervals on a time-scale

plane. Positive or negative peaks in time-scale representations were called modulus maxima. Their values indicated the edge slope and width.

Shih and Tseng [21] combined gradient-based edge detection and a wavelet based multi-scale edge tracking to extract edges. The proposed contextual filter detects edges from the finest scale gradient images and then, the edge tracker refines the detected edges on the multi-scale gradient images.

Statistical Methods: This statistical edge detection is data driven, unlike standard methods for edge detection which are model based. For example, Konishi et al. [23] formulated the edge detection as a statistical inference. For any set of edge detection filters, they used pre-segmented images to learn the probability distributions of filter responses conditioned on whether they are evaluated on or off an edge. Edge detection is formulated as a discrimination task specified by a likelihood ratio test on the filter responses. This approach emphasizes the necessity of modeling the image background (the off-edges). They represented the conditional probability distributions non-parametrically and illustrated them on two different data sets of images. Multiple edges cues including multiple scales were combined by using their joint distributions. Hence, this cue combination is optimal in the statistical sense.

Machine Learning Based Methods: These are approaches depending on machine learning. These include works by Wu et al. [24] where they introduced a fast multilevel fuzzy edge detection algorithm that realizes the fast and accurate detection of the edges from the blurry images. The algorithm first enhances the image contrast by means of the fast multilevel fuzzy enhancement (FMFE) algorithm using the simple transformation function based on two image thresholds. Second, the edges are extracted from the enhanced image by the two-stage edge detection operator that identifies the edge candidates based on the local characteristics

of the image and then determines the true edge pixels using the edge detection operator based on the extremum of the gradient values. They demonstrated that the algorithm can extract the thin edges and remove the false edges from the image, which leads to its better performance than the Sobel operator, Canny operator, traditional fuzzy edge detection algorithm, and other multilevel fuzzy edge detection algorithms. In another study, Lu et al. [18] proposed a fuzzy neural network system for edge detection and enhancement by recovering missing edges and eliminating false edges caused by noise. The algorithm was comprised of three stages, namely, adaptive fuzzification by fuzzifying the input patterns, edge detection by a three-layer feed forward fuzzy neural network, and edge enhancement by a modified Hopfield neural network. The typical sample patterns were first fuzzified and applied to train a fuzzy neural network. The trained network was able to determine the edge elements with eight orientations. Pixels having high edge membership were traced for further processing. Based on constraint satisfaction and the competitive mechanism, interconnections among neurons were determined in the Hopfield neural network. A criterion was provided to find the final stable result that contains the enhanced edge measurement.

Contextual Methods: Yu and Chang [22] suggested an adaptive edge detection approach based on context analysis. The proposed approach uses the information from predictive error values produced by the gradient-adjusted predictor (GAP) to detect edges. GAP uses a context, which is a combination of the intensity values of already processed neighboring pixels defined by a template, to produce the predictive values. The context in the casual template of GAP is used to analyze whether the current pixel is an edge point or not.

Line edge detectors: As mentioned earlier, line edges correspond to local maxima of intensity function in the image and are of great use in the identification of image features, such as roads and rivers in remote sensing images, as well as the contactless paper counting.

Most of line edge detectors are limited to thinning algorithms, and designed for binary images and a few for grey images. The main problem is that they usually yield edges which are not located accurately enough and they do not perform well in complex images such as remote sensing images.

Haralick [35] proposed an algorithm based on polynomial fitting. The image was fitted by a linear combination of discrete bases of Tchebychev's polynomial of order less than or equal to three. Lines occur at pixels having zero-crossings of the first directional derivative taken in the direction that maximizes the second directional derivative. Giraudon [36] proposed an algorithm for detecting a line at a negative local maximum of the second derivative of the image, rather than a zero-crossing of the first derivative. He estimated the second derivative by convolving the image with the difference of two Gaussians having close scales. The search for a negative maximum is performed along the gradient direction. The main problem with Giraudon's detector comes from the use of the gradient since at the peak point, the gradient value is too small to be used. Using a 1D ideal roof model and Canny's criteria, Ziou [37] derived an optimal line detector. Koundinya and Chanda [38] proposed an algorithm based on combinatorial search. The basic idea behind this algorithm is to locate lines that maximize an ad-hoc confidence measure. The confidence measure of a candidate pixel is proportional to the number of pixels in its vicinity having a different grey intensity than the candidate pixel. They examined three strategies for combinatorial search: conventional tracking, best-first, and depth-first. According to the results, the best-first strategy seemed to provide more complete edges.

2.3.2. Overview of Color Edge Detection Methodologies

High level image processing applications, such as object recognition, segmentation, image coding, and robot vision, depend on the accuracy of edge detection since edges contain

essential image information. In a monochrome image, an edge usually corresponds to object boundaries or changes in physical properties such as illumination or reflectance. This definition is more elaborate in the case of multispectral color images since more detailed edge information is expected from color edge detection. According to psychological research on the human visual system, color plays a significant role in the perception of boundaries. Monochrome edge detection may not be sufficient for certain applications since no edges will be detected in gray value images when neighboring objects have different hues but equal intensities. Objects with such boundaries are treated as one big object in the scene. Since the capability to distinguish between different objects is crucial for applications such as object recognition and image segmentation, the additional boundary information provided by color is of paramount importance. Color edge detection also outperforms monochrome edge detection in low contrast images. There is thus a strong motivation to develop efficient color edge detectors that provide high quality edge maps. Shu-Yu Zhu, Konstantinos N., and Anastasios N. (1999) suggested comprehensive analysis of edge detection in color image processing [16]. Here various approaches to edge detection for color images, including techniques extended from monochrome edge detection as well as vector space approaches are examined. In particular, edge detection techniques based on vector order statistic operators and difference vector operators are studied in detail. Numerous edge detectors are obtained as special cases of these two classes of operators. First it introduces some important concepts by comparing gray scale/monochromatic and color/multispectral edge detection methods and secondly it overviews the two categories of color edge detection methods with discussion of the sub categories.

2.3.2.1. Serial (synthetic) Methods or Monochrome Based Methods

In a monochrome image, an edge is defined as an intensity discontinuity. In the case of color images, the additional variation in color must also be considered. Early approaches to color

edge detection are extensions of monochrome edge detection. These techniques are applied to the three color channels independently and then the results are combined using certain logical operation (image decomposition and image recombination). The image recombination step can be inserted at different places in the edge detection pipeline, as shown in Fig. 2.8. According to the nature of recombination, Ruzon and Tomasi [40] classified the synthetic methods as: output fusion methods [39, 41-46] and multidimensional gradient methods [47-52].

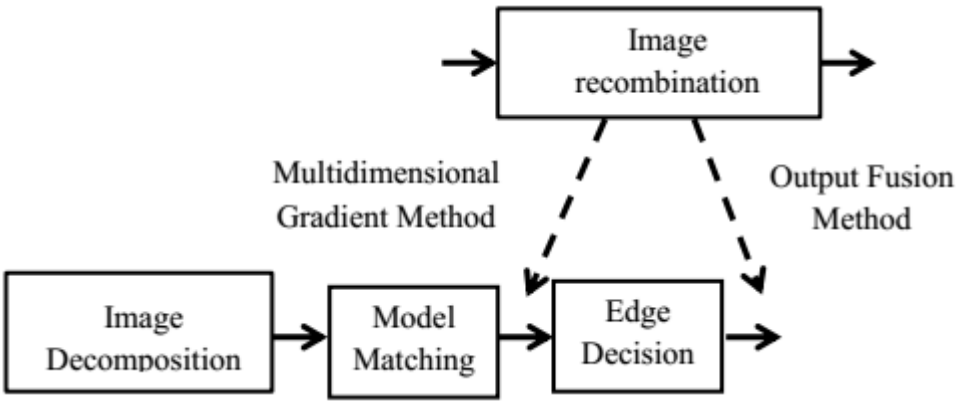

Figure 2.8: Edge detection pipeline for synthetic methods.

Output Fusion Methods

These are illustrated in Table 2.1. The first such method was proposed by Nevatia in 1977 [19]. A number of output fusion methods for color edge detection have been proposed since then. These methods vary in terms of usage of different color spaces, edge detection operators and the fusion criteria.

Multidimensional gradient methods

These monochromatic color edge detection methods make a single estimate of both the orientation and strength of an edge at a point. The detection pipeline is illustrated in Fig. 2.9.The first color edge detector belonging to this category was proposed by Robinson [47] in 1977. Various methods belonging to this category have evolved since then. These methods

differ in terms of how gradients of the image components are combined into one. The methods along with the techniques used to find and combine gradients are listed in Table 2.2.

Table 2.1: Some of the significant output fusion color edge detection methods [54].

Method	Year	Color Space	Edge Detection Operator	Fusion Criterion
Nevatia	1977	YCbCr	Hueckel operator	Same Orientation
Shiozaki	1986	RGB	Entropy operator	Weighted Summation
Hedley and Yan	1992	RGB	Sobel operator	Summation
Carron and Lambert	1994	HIS	Sobel operator	Weighted Summation and Trade-off parameter between Hue and Intensity
Fan et. al	2001	YUV	Second-order gradient, Entropy based threshold	Logical OR
Cabani et. al	2006	RGB	Basic declivity operator	Shortest of basic declivities in the corresponding R, G and B layers
Niu and Li	2006	HSV	Direction Information	Weighted Summation
Chen and Chen	2010	RGB	Improved Sobel operator	Weighted sum and adaptive thresholding using Otsu method

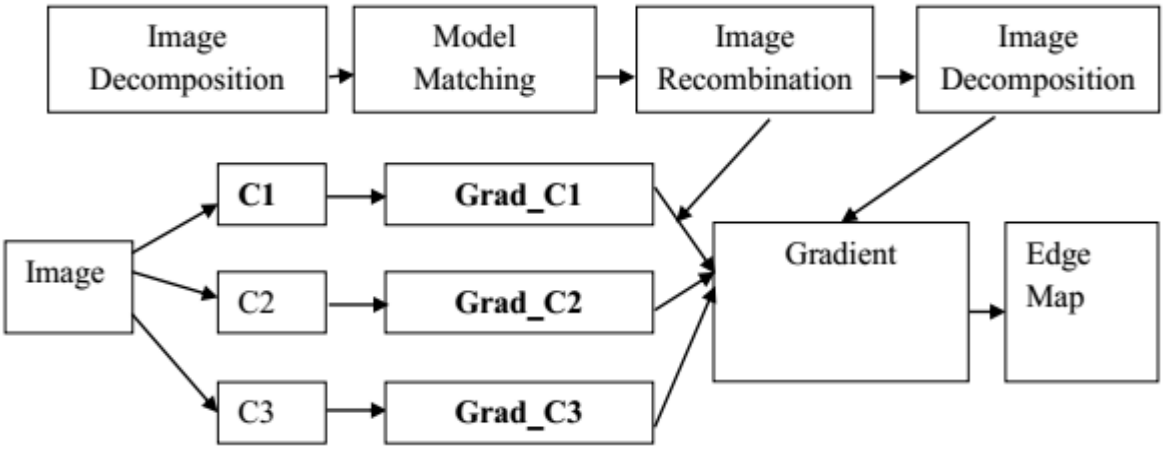

Figure 2.9: Edge detection pipeline for multidimensional gradient methods.

It can be concluded that the monochromatic or synthetic color edge detection method is simple and produces better output than the traditional gray scale edge detection method. But the main drawback is how to combine the channels and the final output is highly dependent on the color space used.

Problem with the Preceding Approaches

All the above approaches fail to take into account the correlation among the color channels. As a result, they are not able to extract certain crucial information conveyed by color. For example, they all tend to miss edges that have the same strength but in opposite direction in two of their color components. As a solution to this vital issue, approaches that treat color pixels as vectors have been proposed in the literature. Hence, vector space approaches [16].

Table 2.2: Multidimensional gradient methods for color edge detection [54].

Method	Year	Gradient Operator	Combination Method
Robinson	1977	24-directional derivatives	Maximum of all the gradients
Zenzo	1986	Sobel gradient	Tensor of gradients: Sum of gradients, Root Mean Square (RMS) of gradients, Maximum of gradients
Cumani	1991	Second order derivatives	Eigen vector approach
Drewniok	1994	Canny edge operator	Integration of information from various channels in a well-founded way. Integration of Correlated information by averaging and integration of uncorrelated information by simple inclusion
Chapron	1997	Canny-Deriche gradient	Neyman-Pearson optimal decision rule
Soumya Dutta	2009	Directional masks	Weighted Summation

2.3.2.2. Vector Space Approaches

Color images can be viewed as 2-D three-channel vector fields, which can be characterized by a discrete integer function $f(x, y)$. The value of this function at each point is defined by a 3-D vector in a given color space. In the RGB color space, the function can be written as $f(x, y) = (R(x, y), G(x, y), B(x, y))$, where (x, y) refers to the spatial dimensions in the 2-D plane. Most existing edge detection algorithms use either first or second difference between neighboring pixels for edge detection [16]. A significant change gives rise to a peak in the first derivative and zero-crossing in the second difference. Some of these operators are considered as follows.

a. Vector Gradient Operators

The vector gradient operator employs the concept of a gradient operator, except that instead of scalar space the operator operates in a 2-D three-channel color vector space. This method can be applied to color edge detection in many different ways but, as illustrated below, two are of more interest. One simple approach is to employ 3×3 window centered on each pixel and then obtain eight distance values $(D_1, D_2, ..., D_8)$ by computing the Euclidean distance between the center vector and its eight neighboring vectors. The vector gradient (g) is then chosen as [16]:

$$g = \max(D_1, D_2, ..., D_8). \tag{2.16}$$

The second approach employs directional operator as follows: The image be a vector function $f(x, y) = (R(x, y), G(x, y), B(x, y))$, and let $r, g,$ and b be the unit vectors along the $R, G,$ and B axes, respectively. The horizontal and vertical directional operators can be defined as:

$$u = \frac{\partial R}{\partial x} r + \frac{\partial G}{\partial x} g + \frac{\partial B}{\partial x} b, \tag{2.17}$$

$$v = \frac{\partial R}{\partial y} r + \frac{\partial G}{\partial y} g + \frac{\partial B}{\partial y} b, \tag{2.18}$$

$$g_{xx} = u.u = \left|\frac{\partial R}{\partial x}\right|^2 + \left|\frac{\partial G}{\partial x}\right|^2 + \left|\frac{\partial B}{\partial x}\right|^2, \tag{2.19}$$

$$g_{yy} = v.v = \left|\frac{\partial R}{\partial y}\right|^2 + \left|\frac{\partial G}{\partial y}\right|^2 + \left|\frac{\partial B}{\partial y}\right|^2, \tag{2.20}$$

$$g_{xy} = \frac{\partial R}{\partial x}\frac{\partial R}{\partial y} + \frac{\partial G}{\partial x}\frac{\partial G}{\partial y} + \frac{\partial B}{\partial x}\frac{\partial B}{\partial y}. \tag{2.21}$$

Then the maximum rate of change of f and the direction of the maximum contrast can be calculated as:

$$\theta = \frac{1}{2}\arctan\frac{2g_{xy}}{g_{xx} - g_{yy}} \tag{2.22}$$

$$F(\theta) = \frac{1}{2}\left[\left(g_{xx} + g_{yy}\right) + \cos 2\theta\left(g_{xx} - g_{yy}\right) + 2g_{xy}\sin\theta\right] \tag{2.23}$$

Edges can be obtained by thresholding $\left[F(\theta)\right]^{1/2}$. The image derivatives along the x and y directions can be computed by convolving the vector function f with two spatial masks as follows:

$$\frac{\partial f_i}{\partial x} \cong \frac{1}{6}\begin{bmatrix} -1 & 0 & 1 \\ -1 & 0 & 1 \\ -1 & 0 & 1 \end{bmatrix} * f_i, \frac{\partial f_i}{\partial y} \cong \frac{1}{6}\begin{bmatrix} 1 & 1 & 1 \\ 0 & 0 & 0 \\ -1 & -1 & -1 \end{bmatrix} * f_i \text{ for } i = 1,2,3 \tag{2.24}$$

Compared to the gradient operator extended from monochromatic edge detection, more color information can be extracted using the vector gradient operator since it considers the vector nature of the color image. The method has, however, two major limitations: sensitivity to small texture variations and sensitivity to Gaussian and impulse noises.

b. **Directional Operators**

Directional vector operators were proposed to detect the location and orientation of edges in color images [16]. In this approach, a color $c(r,g,b)$ is represented by a vector c in color space. Similar to the well- known Prewitt operator shown below:

$$\Delta H = \frac{1}{3}\begin{pmatrix} -1 & 0 & 1 \\ -1 & 0 & 1 \\ -1 & 0 & 1 \end{pmatrix}, \quad \Delta V = \frac{1}{3}\begin{pmatrix} -1 & -1 & -1 \\ 0 & 0 & 0 \\ 1 & 1 & 1 \end{pmatrix} \tag{2.25}$$

the row and column of directional operators (i.e. in the horizontal (ΔH) and vertical (ΔV) direction), each having one positive and one negative component. For operators of size $(2w+1)\times(2w+1)$ the general configuration is the following:

$$\Delta H = \begin{bmatrix} H_- & 0 & H_+ \end{bmatrix}, \Delta V = \begin{bmatrix} V_- \\ 0 \\ V_+ \end{bmatrix} \tag{2.26}$$

where the parameter w is a positive integer. These positive and negative components are convolution kernels, denoted by V_-, V_+, H_- and H_+, whose outputs are vectors corresponding to the local average colors. The major limitation of this method is that as the parameter w decreases, the operator sensitivity to noise increases as well as sharp edge detection also decreases.

c. **Compound Edge Detectors**

The simple color gradient operator can also be used to implement compound gradient operators. A well-known example of a compound operator is the derivative of Gaussian (D*G*) operator. In this case, each channel of the color image is initially convolved with a Gaussian

smoothing function $G(x, y, s)$, where s is the standard deviation, and, after then this gradient operator is applied to the smoothed color image to detect edges. The major limitation of this method is that it is sensitive to impulsive noise.

d. **Entropy operator**

The entropy operator is employed for both monochrome and color images. It yields a small value when the chromaticity in the local region is uniform and a large value when there are drastic changes in the chromaticity. The entropy in a processing window (i.e., 3x3) centered on vector $v_o = (r_o, g_o, b_o)$ is defined as:

$$H = q_R H_R + q_G H_G + q_B H_B \tag{2.27}$$

where H_R, H_G, and H_B, denote the entropies in the R, G and B directions, respectively, and

$$q_R = \frac{r_o}{r_o + g_o + b_o},\ q_G = \frac{g_o}{r_o + g_o + b_o},\quad q_B = \frac{b_o}{r_o + g_o + b_o} \tag{2.28}$$

Let $X_{0,} X_1, ..., X_{N,} (X = R, G, B)$ denote the values in each corresponding channel inside the processing window, and H_x is defined as:

$$H_x = \frac{-\sum_{i=1}^{N} px_i \log(px_i)}{\log(N)} \text{ where } px_i = \frac{X_i}{\sum_{j=1}^{N} X_j} \tag{2.29}$$

The major limitation of the method is its sensitivity to noise**.**

e. Second Derivative Operators

Cumani suggested a more sophisticated approach that involves second derivative operator [49]. The edge points are determined by computing zero crossing of the directional derivatives. The ambiguity of the gradient direction in the above method causes some difficulties in locating edge points. Cumani suggested the sub pixel technique with bilinear interpolation to solve the problem. Alshatti and Lambert suggested a modification in solving the ambiguities by estimating the eigenvector, which can avoid the computationally costly sub pixel approximation [53]. Other techniques have also been proposed to reduce the complexity of the Cumani operator. Similar to the vector gradient operator, the second-order derivative operator is very sensitive to texture variations and impulsive noise, but it produces thinner edges. The regularizing filter applied in this operator causes a certain amount of blurriness in the edge map.

Vector Order Statistic Operators

This family of edge detection methods are based on order statstics. It has played an important role in monochrome or grayscale image processing particularly in edge detection. This approach was inspired by the morphological edge detectors that have been proposed for monochromatic images. This class of color edge detectors is characterized by linear combinations of the sorted vector samples. Different sets of coefficients of the linear combination give rise to different edge detectors that vary in performance and efficiency. The primary step in order statistics is to arrange a set of random variables in ascending order according to certain criteria. In color space, since we are dealing with 2-D, multichannel variables, there is no universal way of defining an ordering. A number of ways have been proposed to perform multivariate data ordering and they can be classified into marginal ordering (*M*-ordering), reduced aggregate ordering (*R*-ordering), partial ordering (*P*-ordering), and conditional ordering (*C*-ordering). In *M*-ordering, the ordered vectors do not

correspond to the original vectors, and *P*-ordering is difficult to implement for digital image processing. *C*-ordering considers only one color component. *R*-ordering is hence more appropriate for color image processing. *R*-ordering reduces each multichannel variable to a scalar value according to a distance criterion. Let the image vectors in a window w denoted by $X_i, i = 1,2,...,n$ and $D(X_i, X_j)$ be a measure of distance between vectors X_i and X_j .The reduced scalar quantity associated with X_i is defined as:

$$d_i = \sum_{k=1}^{n} D(x_i, x_k), i = 1,2,...,n. \tag{2.30}$$

The arrangement of d_i in ascending order $d^{(1)} \le d^{(2)} \le ..., d^{(n)}$ corresponds to the same ordering to the multivariate variables $X^{(1)} \le X^{(2)} \le ... \le X^{(n)}$. In the ordered sequence, X^1 is the vector median and vectors appearing at high ranks are referred to as outliers because they diverge the most from the data population. The vector range (VR) is the simplest way of color edge detection method that works based on order statistics. The deviation of the vector outlier can be expressed in the highest rank from vector median in w as follows.

$$VR = D\left(X^{(n)}, X^{(1)}\right) \tag{2.31}$$

where VR is small in a uniform area since all vectors are close together, and it gives large output when discontinuities exist. Edges can be obtained by thresholding the VR outputs.

Difference Vector Operators

The class of difference vector (DV) operators can be viewed as first derivative like operators. This group of operators is extremely effective from the point of view of the computational aspects of the human visual system. In this approach, each pixel represents a vector in the RGB color space, and a gradient is obtained in each of the four possible directions (0, 45, 90,

and 135 degrees) by applying convolution kernels to the pixel window. Then a threshold can be applied to the maximum gradient vector to locate edges [6]. The gradients are defined as:

$$\begin{aligned}
&|\nabla f|_{0}\,\text{deg} = \|Y_{0}\,\text{deg} - X_{0}\,\text{deg}\|,\\
&|\nabla f|_{90}\,\text{deg} = \|Y_{90}\,\text{deg} - X_{90}\,\text{deg}\|\\
&|\nabla f|_{45}\,\text{deg} = \|Y_{45}\,\text{deg} - X_{45}\,\text{deg}\|,\\
&|\nabla f|_{135}\,\text{deg} = \|Y_{135}\,\text{deg} - Y_{135}\,\text{deg}\|,\\
&DV = \max\left(|\nabla f|_{0}\,\text{deg}, |\nabla f|_{90}\,\text{deg}, |\nabla f|_{45}\,\text{deg}, |\nabla f|_{135}\,\text{deg}\right),
\end{aligned} \tag{2.32}$$

where $\|.\|$ denotes the L2 norm, and X and Y are three dimensional vectors used as convolution kernels.

2.4. Summary of Vectorial Edge Detection Approaches

The vectorial edge detection approches discussed above treat color images as 2-D three-channel vector fields. However, these edge detection algorithms use either first or second difference between neighboring pixels for edge detection. A significant change gives rise to a peak in the first derivative and zero-crossing in the second difference. As a result, only edges with high intensity value can be detected very well. An effective color edge detection requires not just a vectorial scheme but a more systematic manipulation of the inter correlation information that is embedded among the monochromes (vector components) that make up the color image.

The intension of this thesis work is to develop an algorithm which applies systemic manipulation of color bands holistically so that it keeps the inter correlation information of vector components and able to detect edges of high degree of difficulty color images and finally apply to MP-MRI medical images.

3. Multi-Parametric Magnetic Resonance Imaging and Brain Tumours

3.1. Medical Imaging Modalities

Today, the diagnosis of a patient is rarely done without the use of imaging technology. Medical imaging allows us to look inside the body, without resorting to invasive methods. Not only more comfortable and safe for the patient, imaging also allow views of anatomy and physiology that cannot be obtained by any other means. Since the discovery of X-rays by Roontgen, the last 100 years have seen a veritable boom in medical imaging modalities and technology. X-rays together with CT, ultrasound, MRI, SPECT and PET allow the physician to examine the patient in a manner beyond imagination only 50 years ago. In general, imaging can address two issues: structure and function. One can either view structures in the body and thus image anatomy, or view chemical or dynamic processes, and image biochemistry and physiology. Structural imaging techniques include X-rays, CT and MRI. It is the role of fMRI, SPECT and PET to view the biochemical and physiological processes inside the body (e.g. brain) [55]. Here for this thesis work the medical imaging modality used is MRI that provides the most detailed anatomical information of all the structural imaging modalities.

3.2. Brain MRI

Presently, examinations of the brain are the second most commonly requested MR study following spine examinations (Radiology Dept. Statistics, 2001) [56].

Indications that we can get from MRI

- ✓ Look for the cause of headaches.
- ✓ Help diagnose a stroke or blood vessel problems in the head. Problems with blood vessels may include an aneurysm or abnormal twisted blood vessels that are present at birth (this is called an arteriovenous [AV] malformation).

- ✓ Check blood flow or blood clots to the brain. MRI can show bleeding in or around the brain.
- ✓ Check symptoms of a known or suspected head injury.
- ✓ Check symptoms such as change in consciousness, confusion, or abnormal movements. These symptoms may be caused by brain diseases, such as Huntington's disease, multiple sclerosis (MS), Parkinson's disease, or Alzheimer's disease.
- ✓ Check for "water on the brain" (hydrocephaly).
- ✓ Look for tumors, infections, an abscess, or conditions of the brain or brain stem, such as encephalitis or meningitis.
- ✓ Look for problems of the pituitary gland (macro adenoma and micro adenoma).
- ✓ Investigate or follow a finding seen on another test.

Suggested Protocol for Routine Brain Imaging with Planning Method

Sagittal SE/FSE T1, Axial SE/FSE T2, Coronal SE/FSE T2, Axial FLAIR, for periventricular or cord lesions such as MS plaques and Axial DWI, for investigation of early stroke. Coil used: Head coil and Patient position: supine, head first (in) and should be straight with the horizontal alignment light passes through the nasion (the intersection of the frontal bone and two nasal bones of the human skull) [56] (see Fig. 3.1).

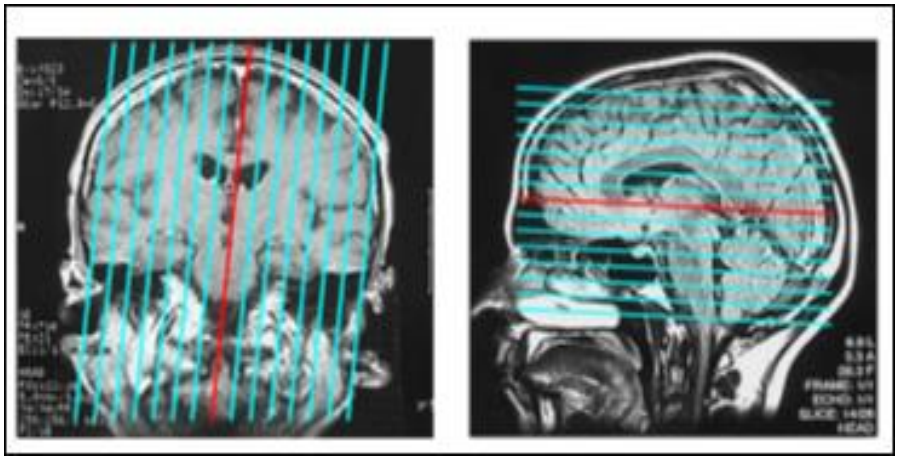

Figure 3.1: Sagittal SE/FSE T1 and Axial SE/FSE T2 (right).

3.2.1. Types of MRI sequences

An MRI sequence is a number of radiofrequency pulses and gradients that result in a set of images with particular appearance. This section presents a simplified approach of recognizing and thinking about common MRI sequences which include the followings [56]:

a. T1 Weighting
b. T2 Weighting
c. Proton Density Weighting
d. ADC (Apparent diffusion coefficient)
e. DWI (Diffusion weighted sequences)

a. T1 Weighted MRI

A T1 weighted image is an image whose contrast is predominantly due to the differences in T1 recovery times of tissues. MRI scans can be acquired with various types of contrast. T1-weighted images are weighted according to the so-called spin-lattice relaxation time (T1) of the protons that give rise to the MRI signals; such images provide good contrast between grayed white matter. T1 weighted images are typically used for anatomic information, providing also high sensitivity for paramagnetic contrast media that can show pathology, fat, fluids with high protein content and sub-acute hemorrhage.

Signal Intensities in T1 weighted Images: Tissues with short T1 relaxation times such as fat, are bright (high signal), because they recover most of their longitudinal magnetization during the TR and therefore more magnetization available for next RF pulse. Tissues with long T1 relaxation times such as water are dark (low signal) [56].

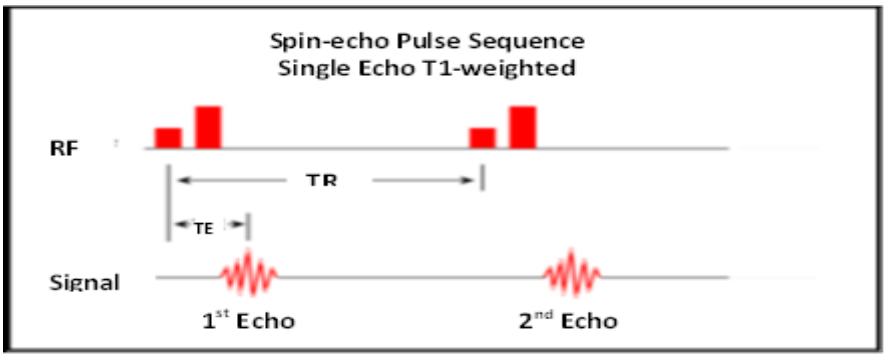

Figure 3.2: Signal intensities in T1 weighted images.

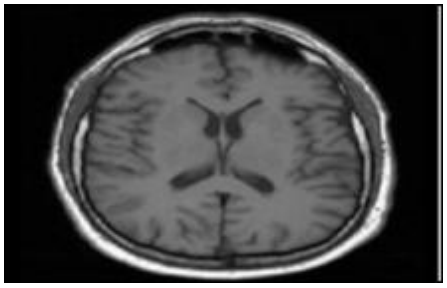

Figure 3.3: Typical T1 weighted image.

b. T2 Weighted MRI

A T2 weighted image is an image whose contrast is predominantly due to the differences in T2 decay times of tissues. T2 weighted scans use a spin echo (SE) sequence, with long TE and long TR. They have long been the clinical workhorse as the spin echo sequence is less susceptible to in-homogeneities in the magnetic field. They are particularly well suited to edema as they are sensitive to water content (edema is characterized by increased water content). T2 weighted images offer high sensitivity to most pathologic processes as most pathology have increased water content and are therefore bright on T2 weighted images.

A prolongation of T2, which provides high signal intensities on long TR and long TE images, is seen with edema, infarction, demyelination, infection, neoplasm and most fluid collections.

Signal Intensities in T2 weighted Images [56]:

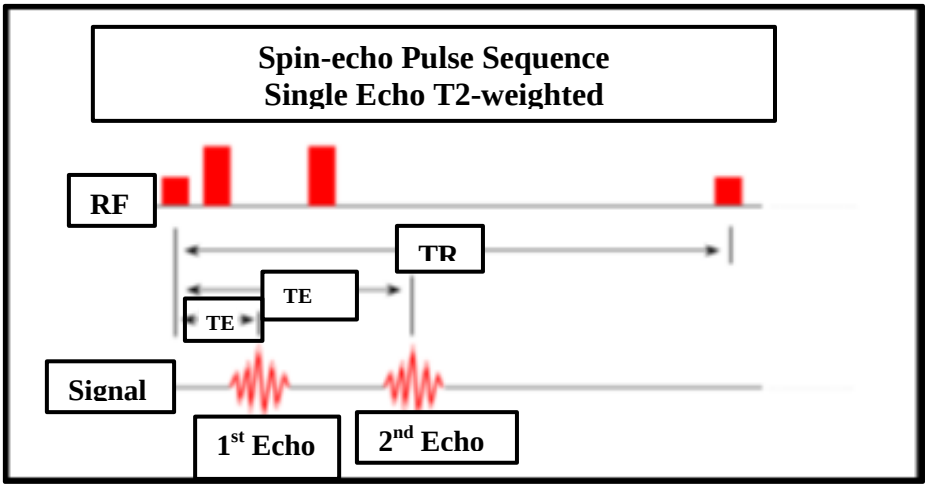

Figure 3.4: Signal intensities in T2 weighted images.

Tissues with short T2 decay time such as Fat, are dark (low signal), because they lose most of their coherent transverse magnetization during the TE period. Tissues with long T2 decay time such as water are bright (high signal).

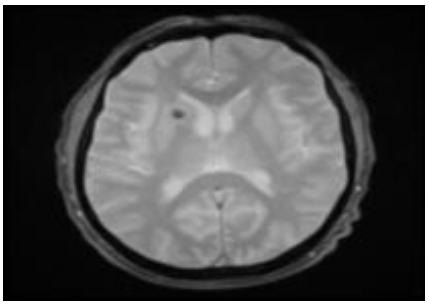

Figure 3.5: A typical T2 weighted image.

T2* Weighted MRI: T2* (pronounced "T2 star") weighted scans use a gradient echo (GRE) sequence, with long TE and long TR. The gradient echo sequence used does not have the extra refocusing pulse used in spin echo so it is subject to additional losses above the normal T2 decay (referred to as T2'), these taken together are called T2*. This also makes it more prone to susceptibility losses at air/tissue boundaries, but can increase contrast for

certain types of tissue, such as venous blood. Table 3.1 summarizes major differences between T2 and T2* parameters [56].

Table 3.1: The difference between T2 and T2*.

T2	T2*
1. Time constant for loss of (transverse magnetization) signal in a spin echo MRI sequence. 2. Is the transverse relaxation time.	1. Time constant for loss of (transverse magnetization) signal in a gradient echo MRI sequence. 2. Is the effective time of FID (free induction decay).

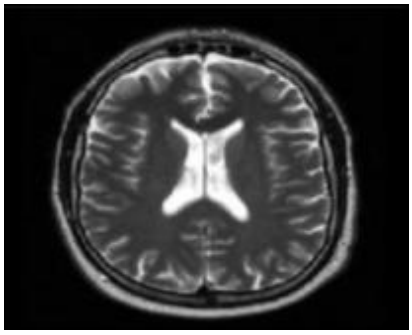

Figure 3.6: A typical T2* weighted image.

Fluid Attenuated Inversion Recovery (FLAIR): Fluid Attenuated Inversion Recovery (FLAIR) images are T2-weighted with the CSF signal suppressed. This pulse sequence is used to null signal from fluids. For example, it can be used in brain imaging to suppress Cerebrospinal Fluid (CSF) so as to bring out the periventricular hyper intense lesions, such as multiple sclerosis (MS) plaques. By carefully choosing the inversion time TI (the time between the inversion and excitation pulses), signal from any particular tissue can be suppressed (see Fig. 3.7).

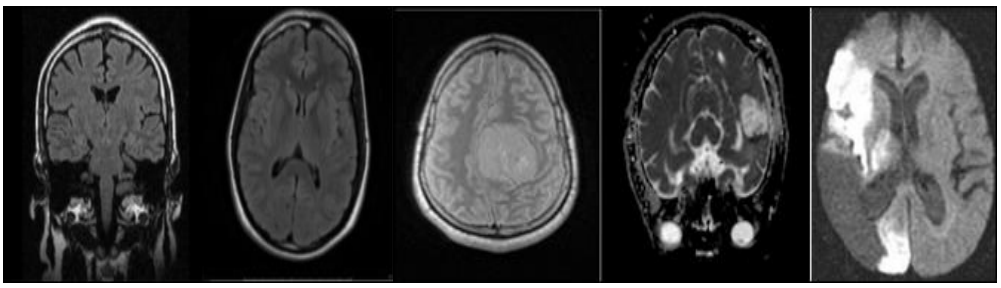

Figure 3.7: Typical FLAIR (coronal (1st), axial (2nd)), PD (3rd), ADC (4th), and DWI images.

c. Proton Density (PD) Weighting

It is the tissues with the higher concentration or density of protons (hydrogen atoms) which produce the strongest signals and appear the brightest on the image. Proton density images have been extensively used for brain imaging; however they have largely been replaced by FLAIR. PD however continues to offer excellent signal distinction between fluid hyaline cartilage and fibrocartilage making this sequence ideal in assessment of joints (see Fig. 3.7).

d. Apparent diffusion coefficient (ADC)

Apparent Diffusion Coefficient (ADC) maps represent the actual diffusion values of the tissue without T2 effects. They are therefore much more useful, and objective measures of diffusion values can be obtained, however they are much less pretty to look at (see Fig. 3.7).

e. Diffusion weighted sequences (DWI)

Diffusion weighted imaging assess the ease with which water molecules move around within a tissue (mostly representing fluid within the extracellular space) and give insights into cellularity (e.g. tumours), cell swelling (e.g. ischemia) and edema (see Fig. 3.7).

3.3. Multiparametric-magnetic resonance imaging (MP-MRI) and analysis

As briefly discussed in section 3.3.1 above, no doubt at all that the individual sequence of MRI are able to covey useful information. Recent studies however proved that analyzing each component/MRI parameter of such images serially has a main drawback in that it misses the

information as to how the different parameters are correlated to each other. Multiparametric Magnetic Resonance Imaging (MP-MRI) can be obtained in most centers that operate state-of-the-art 1.5-Tesla (1.5T) or 3T scanners. The term "multiparametric" refers to the multiple MRI sequences that are required to make the diagnosis, which differs from other MRI scans in which the diagnosis usually depends on one essential MRI sequence. MP-MRI has shown promising results in diagnosis, localization, risk stratification and staging of clinically significant prostate, brain and such a like cancers. Combinations of T1-W, T2-W imaging, diffusion imaging, perfusion (dynamic contrast-enhanced imaging) and spectroscopic imaging have been used in MP-MRI assessment of cancers. This section discusses the current role of MP-MRI in prostate, brain and breast cancer management.

Currently, the diagnostic pathway for prostate cancer detection is by the use of prostate-specific antigen (PSA) screening followed by random biopsy [57]. This encourages the development of new imaging methods for prostate cancer. Screening methods based on serum PSA followed by random biopsies tend to over diagnose small indolent tumors. Meanwhile, larger, aggressive lesions that are outside the typical biopsy template may not be found with the strategy of PSA screening and random biopsy. This combination of PSA screening and random biopsy has yielded disappointing clinical outcomes. Thus, there is increasing recognition of the potential value of adding an imaging method to guide biopsy, thereby detecting larger tumors that are more likely to be clinically significant while reducing the over diagnosis of smaller indolent cancers that are below the detection threshold of imaging. MP-MRI has emerged as the most promising of the imaging modalities for this task. Compared with serum PSA screening and random biopsy, MP-MRI with image-guided biopsy of the prostate enables direct assessment of the location, size, and stage of distinct lesions within the prostate. T2-weighted (T2W), Dynamic contrast enhanced (DCE) and diffusion weighted (DW) MRI have demonstrated their potential value in distinguishing

malignant from benign prostate tissue, but none of them used alone is capable of optimally characterizing tumors in the prostate [58].

MP-MR imaging has also shown promises for detection and characterization of breast lesions [59, 60]. Different literatures have proved as mammography is an effective tool for early screening and detection of breast cancer. However, the technique has limited specificity (32-64%) and mammography frequently cannot distinguish benign from malignant diseases [61, 62]. The other limitation which is raised by different researchers is that this technique is not able to detect about 10% of cancers due to dense fibro glandular tissue that obscures visualization of the tumor. These limitations led to the use of imaging methods like breast ultrasound which is highly user dependent in the interpretation of breast sonograms. The other promising imaging method is MRI. However, it is unlikely that a single MRI parameter can characterize the complexity of breast tissue. Techniques such as MP-MRI provide a comprehensive data set with potentially more power to diagnose breast diseases than any single measure alone.

These MP-MR images do contribute a lot in identification, segmentation and differentiation of different types of brain tumor, which is the subject of this thesis. Multi-parametric tissue characterization helps to better differentiate between neoplasm (a new and abnormal growth of tissue in a part of the body, especially as a characteristic of cancer), edema (a condition characterized by an excess of watery fluid collecting in the cavities or tissues of the body) and healthy tissue, and to identify tissues that are likely to progress to neoplasm in the future [63]. Other literature demonstrates that multiple MR parameters are combined to one entity and analyzed holistically using higher order Fourier transforms for use in automatic detection and effective segmentation of brain tumors based on principles derived from color image processing [64]. The approach has been implemented in terms of identification of brain tumors in MRI taken from a cohort of patients treated for Glioblastoma multiforme (GBM),

the highest grade and most aggressive of the gliomas. The results obtained show that the idea of combining the information from different MRI techniques goes much beyond what can be achieved by using any single parameter, thus allowing an improved image processing and pattern recognition. This is the basis for this thesis work. The thesis borrows many principles from this particular study and similar other works and tries to elaborate on their applicability in effective edge detection of MP-MR images.

3.4. Some Examples of MR Brain Cases

Multiple sclerosis (ms) (white matter disease): is defined in pathology as a chronic inflammatory disease of the central nervous system, which leads to the formation of multiple focal demyelinated lesions in the white matter. Very similar lesions, as those seen in MS patients, can be induced in models of experimental autoimmune encephalomyelitis (EAE), an autoimmune disease, which is induced by active sensitisation of genetically susceptible animals with brain antigens [65]. In addition, autoreactive T-lymphocytes as well as autoantibodies directed against antigens of the central nervous system can be detected in the circulation of multiple sclerosis patients [66]. For this reason, it is widely believed that multiple sclerosis is an inflammatory autoimmune disease, specifically directed against myelin antigens. The lesions of multiple sclerosis appear as very bright lesions in white matter of the brain (see Fig. 3.23) in T2 weighted images and proton density weighted images.

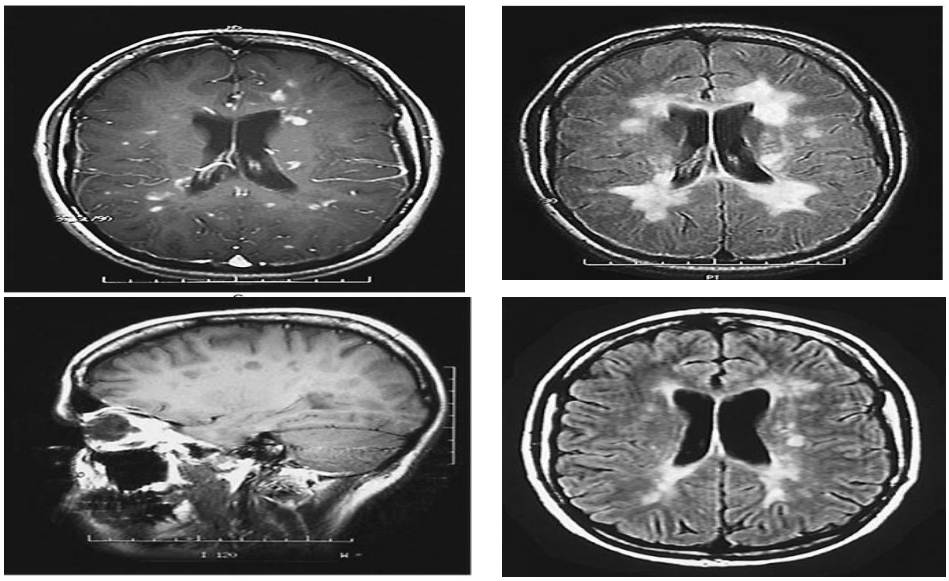

Figure 3.8: Some examples of Multiple sclerosis (ms) (white matter disease).

Stroke: Cerebrovascular disease can be divided into two major categories: ischemic and hemorrhagic stroke. Ischemic stroke accounts for approximately 80% of all strokes and is a result of occlusion of a blood vessel supplying an area of brain, depriving it of glucose and oxygen. Infarct (an area of tissue death that is due to a local lack of oxygen) appears dark on T1-weighted images and bright on T2-weighted images (see Fig.3.24).

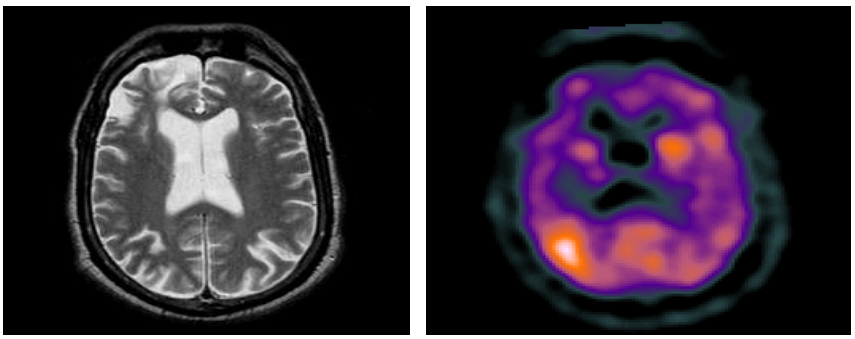

Figure 3.9: Two images of a parietal lobe stroke.

Middle cerebral artery stroke: Middle cerebral artery syndrome is a condition whereby the blood supply from the middle cerebral artery (MCA) is restricted, leading to a reduction of the function of the portions of the brain supplied by that vessel: the lateral aspects of frontal, temporal and parietal lobes, the corona radiata, globus pallidus, caudate and putamen. The MCA is the most common site for the occurrence of ischemic stroke [67].

Depending upon the location and severity of the occlusion, signs and symptoms may vary within the population affected with MCA syndrome. More distal blockages tend to produce milder deficits due to more extensive branching of the artery and less ischemic response. In contrast, the most proximal occlusions result in widespread effects that can lead to significant cerebral edema, increased intracranial pressure, loss of consciousness and could even be fatal [67]. In such occasions, mannitol (osmotic diuretic) or hypertonic saline are given to draw fluid out of the oedematus cerebrum to minimise secondary injury. Hypertonic saline is better than mannitol, as mannitol being a diuretic will decrease the mean arterial pressure and since cerebral perfusion is mean arterial pressure minus intracranial pressure, mannitol will also cause a decrease in cerebral perfusion. Contralateral hemiparesis and hemi sensory loss of the face, upper and lower extremities is the most common presentation of MCA syndrome [67]. Lower extremity function is more spared than that of the faciobrachial region [68]. The majority of the primary motor and somatosensory cortices are supplied by the MCA and the cortical homunculus can, therefore, be used to localize the defects more precisely. Figure 3.25 (right) presents middle cerebral artery stroke.

Cerebral Hemorrhage: A cerebral hemorrhage (also known as a cerebral hematoma) is a type of intracranial hemorrhage (intracranial hematoma) that occurs within the brain tissue (see Fig.3.25 left). It is alternatively called intracerebral hemorrhage. It can be caused by brain trauma, or it can occur spontaneously in hemorrhagic stroke. Non-traumatic intracerebral hemorrhage is a spontaneous bleeding into the brain tissue. Non-traumatic can refer to increased excertion, tension or stress [69]. A cerebral hemorrhage is an intra-axial hemorrhage; that is, it occurs within the brain tissue rather than outside of it.

The other category of intracranial hemorrhage is extra-axial hemorrhage, such as epidural, subdural, and subarachnoid hematomas, which all occur within the skull but outside of the

brain tissue. There are two main kinds of intra-axial hemorrhages: intraparenchymal hemorrhage and intraventricular hemorrhages. As with other types of hemorrhages within the skull, intraparenchymal bleeds are a serious medical emergency because they can increase intracranial pressure, which if left untreated can lead to coma and death. The mortality rate for intraparenchymal bleeds is over 40% [70].

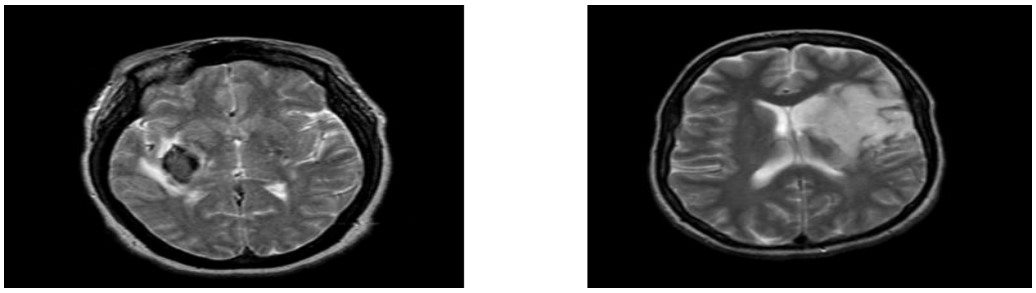

Figure 3.10: Two images of a parietal lobe stroke coupled with an old frontal lobe stroke.

4. Color Medical Image Processing

4.1. Introduction

Image processing is the study of any algorithm that takes a raw image received from cameras/sensors as input to enhance and returns an image or its attributes as an output. Recently, the demand for image processing and its applications in biomedical imaging is increasing. Interest in image processing methods stems from two principal application areas: improvement of pictorial information for human interpretation; and processing of image data for storage, transmission, and representation for autonomous machine perception [72]. In general, image processing covers four main areas: image formation, visualization, analysis, and management [71]. The subjects in this thesis are digital medical images and therefore all discussions in this section are particularly related to digital image processing.

Digital Image Processing

A digital image can be considered as a discrete representation of data possessing both spatial (layout) and intensity (color) information. An image may also be defined as a two-dimensional function, $f(x, y)$ where x and y are spatial (plane) coordinates, and the amplitude of $f(x, y)$ at any pair of coordinates (x, y) is called the intensity or gray level of the image at that point. When x, y and the amplitude values of f are all finite, discrete quantities, we call the image a digital image. Digital image processing refers to processing digital images by means of a digital computer. Note that a digital image is composed of a finite number of elements, each of which has a particular location and value. These elements are referred to as picture elements, image elements, pels, and pixels. Pixel is the term most widely used to denote the elements of a digital image.

Vision is the most advanced of our senses, so it is not surprising that images play the single most important role in human perception. However, unlike humans, who are limited to the visual band of the electromagnetic (EM) spectrum, imaging machines cover almost the entire EM spectrum, ranging from gamma to radio waves. They can operate on images generated by sources that humans are not accustomed to associating with images. Thus, digital image processing encompasses a wide and varied field of applications. In image processing one useful paradigm is to consider three types of computerized processes: low, mid, and high level processes [72]. Low-level processes involve primitive operations such as image preprocessing to reduce noise, contrast enhancement, and image sharpening. A low-level process is characterized by the fact that both its inputs and outputs are images. Mid-level processing on images involves tasks such as segmentation (partitioning an image into regions or objects), description of those objects to reduce them to a form suitable for computer processing, and classification (recognition) of individual objects. A mid-level process is characterized by the fact that its inputs generally are images, but its outputs are attributes extracted from those images (e.g., edges, contours, and the identity of individual objects). Finally, higher-level processing involves "making sense" of an ensemble of recognized objects, as in image analysis, and, at the far end of the continuum, performing the cognitive functions normally associated with vision.

Color Spaces

The use of color in image processing is motivated by two principal factors. First, color is a powerful descriptor that often simplifies object identification and extraction from a scene. Second, humans can discern thousands of color shades and intensities, compared to about only two dozen shades of gray. This second factor is particularly important in manual. (i.e., when performed by humans) image analysis. Color image processing is divided into two

major areas: full-color and pseudo-color processing. In full-color category, images are acquired with a full-color sensor, such as a color TV camera or color scanner. In the pseudo-color, the problem is one of assigning a color to particular monochrome intensity. Until recently, most digital image processing was done by pseudo-color level. However in the last few decades, varieties of color sensors and hardware for processing have become available [72]. The branch of color science concerned with the appropriate description and specification of a color is called colorimetry [75, 76]. Color plays a role on how we perceive and analyze things around us. It is a result of the interaction between the electromagnetic radiation (visible light from 400-700 nm), and the object's surface properties (i.e. reflectance and transmittance) [73]. In the human eye, there are photoreceptors that respond to the incident light for color perception. These are the cones. Cones are sensitive to any of the three primary colors as shown in Fig. 4.1 (Red, Green or Blue) [74].

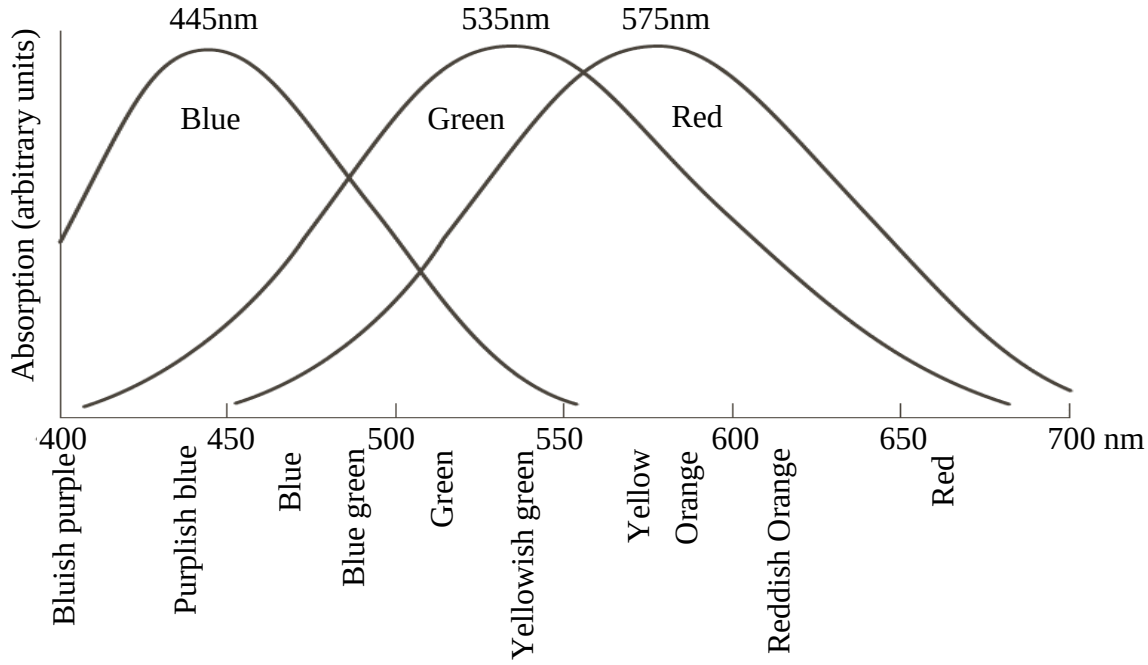

Figure 4.1: Absorption of light by the Red, Green and Blue cons in the human eye as a function of wavelength.

Based on this aspect, a lot of color models were established to quantitatively measure color. Quantitative color measurement is one of the key components in color science, scene

analysis, detection and tracking. Color model literature can be found in the domain of modern sciences, such as physics, engineering, artificial intelligence, computer science, psychology and philosophy. Four basic color model families can be distinguished [77]:

a. **Colorimetric color models**: are based on physical measurements of spectral reflectance. Three primary color filters and a photo-meter, such as the CIE chromaticity diagram [77] usually serve as the initial points for such models.
b. **Psychophysical color models**: are based on the human perception of color. Such models are either based on subjective observation criteria and comparative references (e.g. Munsell color model) or are built through experimentation to comply with the human perception of color (e.g. Hue, Saturation and Lightness (HSL) model).
c. **Physiologically inspired color models**: are based on the three primaries, the three types of cones in the human retina. The Red-Green-Blue (RGB) color space used in computer hardware is the best known example of a physiologically inspired color model.
d. **Opponent color models:** are based on perception experiments, utilizing mainly pairwise opponent primary colors, such as the Yellow-Blue and Red-Green color pairs.

In image processing applications, color models can alternatively be divided into three categories. Namely:

i. **Device-oriented color models:** are associated with input, processing and output signal devices. Such spaces are of paramount importance in modern applications, where there is a need to specify color in a way that is compatible with the hardware tools used to provide, manipulate or receive the color signals.

ii. **User-oriented color models:** are utilized as a bridge between the human operators and the hardware used to manipulate the color information. Such models allow the user to specify color in terms of perceptual attributes and they can be considered an experimental approximation of the human perception of color.

iii. **Device-independent color models**: are used to specify color signals independently of the characteristics of a given device or application. Such models are of importance in applications, where color comparisons and transmission of visual information over networks connecting different hardware platforms are required.

The fundamental assumption behind modern colorimetry theory, as it applies to image processing tasks, is that the initial basis for color vision lies in the different excitation of three classes of photo-receptor cones in the retina. Because of these absorption characteristics of the human eye, colors are seen as variable combinations of the so-called primary colors red (R), green (G), and blue (B), which define a trichromatic space whose basis of primaries are pure colors in the short, medium and high portions of the visible spectrum [75,7 6, 77].

Different category of images (including medical images) can be represented in different color spaces available including: gray spaces, RGB (Red = R, Green = G and Blue =B) spaces, CMYK (Cyan, Magenta, Yellow and Black) spaces and many more. In gray scale images the only colors are shades of gray. Compared to other color images, a gray scale image needs less information to represent each pixel point. In RGB color space a gray color corresponds to equal values of red, green and blue components. The numerical representation of images is relatively simple compared to other color spaces. A gray scale image is stored as an 8-bit integer giving a total of 256 different gray shades (from black to white) with values different in different applications. Often times we use a normalized representation of such integer gray values so that they are bounded between 0 and 1. Commonly used one is 0 for black, 1 for

white and between 0 and 1 for all the remaining gray shades. For hardware that supports only 8-bit images, the color image representation will be limited to gray scale. In many applications it is sufficient to use gray scales to represent images [81]. Color images have at least three components. For example as it is indicated above, the commonly used RGB color image, which is made of the three primary colors red, green and blue, has three components where each perceivable color component is represented by a vector in a three dimensional color space. It is possible to think an RGB color space as a cube in three spaces where each point on the cube corresponds to a vector with three components representing the amount of R, G and B at that particular point. Each color appears in its primary spectral components of red, green, and blue. The model is based on the Cartesian coordinate system and RGB primary values are at the corners of the cube (shown on Fig. 4.2) while secondary colors cyan, magenta, and yellow are at the other corners. Black is at the origin; white is at the furthest corner from the origin. Gray scale (points of equal RGB values) extends from black to white along the line joining these two points (the so called gray line).

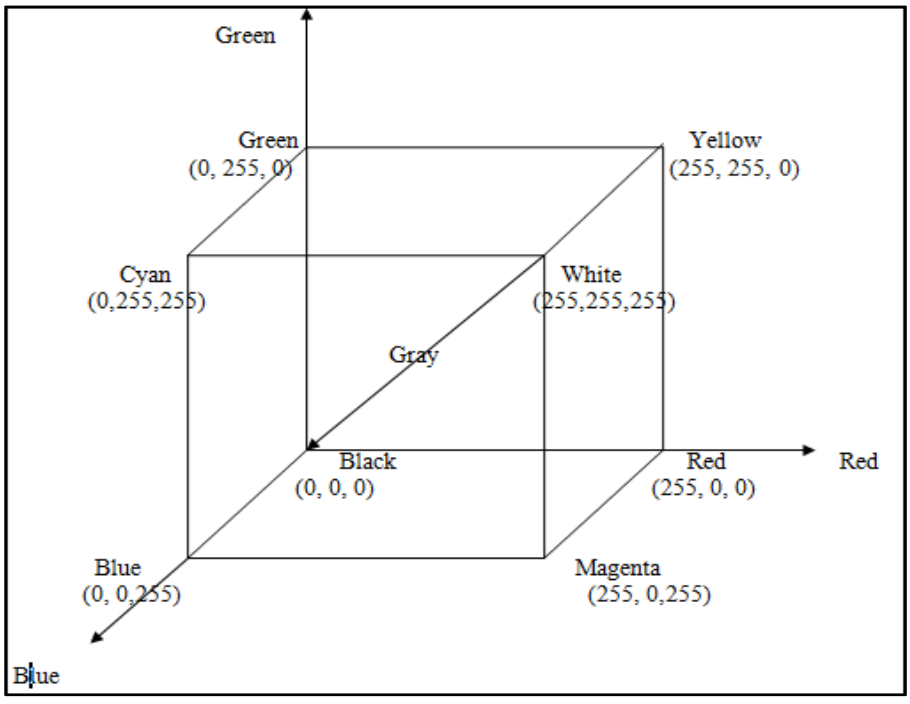

Figure 4.2: Schematic of the RGB color cube. Points along the main diagonal have gray values, from black at the origin to white at point (255,255,255).

All different colors in this model are points on or inside the cube, defined by vectors from the origin. Images in the RGB model consist of three component images; one for each primary. RGB color pixel is of 24-bits (each primary pixel being 8 bits). Total number of colors in 24-bit RGB image is then= $(2^8)^3$ = 16,777,216 (shown on Fig. 4.3).

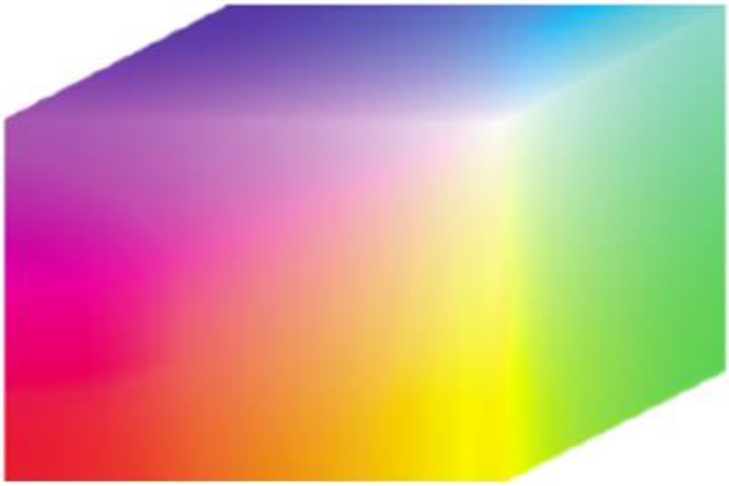

Figure 4.3: RGB 24-bit color cube.

Color Images

Color imaging systems are used to capture and reproduce the scenes that humans see. Imaging systems can be built using a variety of optical, electronic or chemical components. However, all of them perform three basic operations, namely: (i) image capture, (ii) signal processing, and (iii) image formation. Color-imaging devices exploit the trichromatic theory of color to regulate how much light from the three primary colors is absorbed or reflected to produce a desired color. There are a number of ways to acquiring and reproducing color images, including but not limited to:

Photographic film: The film which is used by conventional cameras contains three emulation layers, which are sensitive to red and blue light, which enters through the camera lens.

Digital cameras: Digital cameras use a CCD to capture image information. Color information is captured by placing red, green and blue filters before the CCD and storing the response to each channel.

Cathode-Ray tubes (CRT): CRTs are the display device used in television and computer monitors. They utilize an extremely fine array of phosphors that emit red, green and blue light at intensities governed by an electron gun, in accordance to an image signal. Due to the close proximity of the phosphors and the spatial filtering characteristics of the human eye, the emitted primary colors are mixed together producing an overall color.

Image scanners: The most common method of scanning color images is the utilization of three CCD's each with a filter to capture red, green and blue light reflectance. These three images are then merged to create a copy of the scanned image.

Color printers: Color printers are the most common method of attaining a printed copy of a captured color image. Although the trichromatic theory is still implemented, color in this domain is subtractive. The primaries which are used are usually cyan, magenta and yellow. The amount of the three primaries which appear on the printed media governs how much light is reflected.

4.2. Color Image Analysis

There have been various methods suggested in the literature for use in analysis of both gray scale as well as color images. Some of these methods are structural based; others are statistical based, while others are transforming based. Different hybrid techniques have also been suggested and those are getting more attention. Regarding transform based approaches, the use of Fourier transform and its variants in particular have stimulated various applications in different disciplines. Most integral transforms, like Hartley and Fourier based 2D transforms are, however, primarily built to handle gray scale images which are either real or

complex valued. These gray scale image analysis methods have limited use for images with several color bands. So it is necessary to search analysis methods for colors. There have been various developments in this regard. Below we will revise some methods particularly the traditional monochromatic analysis methods, analysis based on a complex representation of colors and finally the most recent approaches that utilize quaternions, trinions, and the respective integral transforms.

Monochromatic Analysis

As mentioned in the previous sections, one way of analyzing color images is to treat the components as separate monochromatic images. In this way, for example the real and complex valued transforms mentioned above could be used to extract the spectral content available in each color channel. The major drawback of such an approach is that it misses out the correlation information embedded among the different channels of the color images. Finding such correlation information after serial analysis is often not obvious. Another drawback is that the monochromatic analysis essentially results in higher computational costs compared to other holistic approaches. It is sometimes possible to transform a given multi component color image into single component gray scale and do the analysis on a new space. There are instances where this method gives satisfactory results for some applications [78, 79]. Methods that incorporate all color components and the intrinsic inter correlation among the different color components should provide a better approach in handling color images.

Complex Representation of Color Images

Another approach in color image analysis makes use of a representation in the complex space. This is based on converting the original RGB image to HSV color space and considering the hue (H) and saturation (S) components as the phase and the magnitude of the

complex form respectively. As explained in [80], an image h(x, y) represented in the RGB color space with three color bands, R(x, y), G(x, y), and B(x, y), can be converted to HSL color space and represented in cylindrical coordinate system with three color bands, H(x, y), S(x, y) and L(x, y). This can be represented in complex form as:

$$h(x,y) = S(x,y)^{iH(x,y)} \tag{4.1}$$

where the saturation, S(x, y), is the magnitude and the hue, H(x, y), is the phase of the complex form. In this way the standard complex Fourier based transforms can be employed to analyze the color values hue and saturation separated from the intensity. However the intensity is not explicitly represented in this form.

Representation of Color Images in the Hyper-Complex Space

For effective analysis of color images we need a holistic representation technique of all the color channels. In this regard, holistic color image analysis techniques in the hyper-complex space using quaternions and more recently using the three space numbers known by the name trinions have been suggested in the literature [81, 82, 83].

A quaternion has one real and three imaginary components [81]. A quaternion number q can be written as:

$$q = a + ib + jc + kd \tag{4.2}$$

where a, b, c and d are real numbers and i, j and k are orthonormal operators satisfying:

$$i^2 = j^2 = k^2 = ijk = -1, \; ij = k, jk = i, ki = j, ji = -k, kj = -i, ik = -j$$

Quaternions have been used to efficiently represent color images as one object/entity and the respective Fourier transforms defined in the quaternion spaces stimulated several useful

applications in various areas of image analysis. The quaternion Fourier transforms is defined similar to the standard Fourier transform of 2D functions. The non-commutative nature of quaternion multiplication allows for the definition of different types of QFT [83].

The QFT of type I is given by:

$$Q(u,v) = \int_{-\infty}^{\infty}\int_{-\infty}^{\infty} e^{-j2\pi ux} f(x,y) e^{-k2\pi vy} dxdy \tag{4.3}$$

where x and y represent spatial variables while u and v are the wavenumbers (inverse of wavelengths) in the respective directions and $f(x,y)$ is a quaternion. The inverse type I QFT differs from the forward only at the sign of the exponents in the two exponential terms.

A QFT of type II is given by:

$$Q(u,v) = \int_{-\infty}^{\infty}\int_{-\infty}^{\infty} e^{-\mu 2\pi(ux+vy)} f(x,y) dxdy \tag{4.4}$$

where μ is any pure unit quaternion, $\mu^2 = -1$. The formula for the inverse type II QFT differs from the forward one only at the sign of the exponent in the exponential term.

Most color images have, however, three components and one drawback of use of quaternions in representing and analyzing such color images is the extra fourth dimension that quaternions possess which creates redundancy. That means quaternion representation of color images is not unique. A recent work in the field of color image processing aimed to address the issue of this redundancy that we incur using the quaternion formulation. New numbers in the three spaces known by the name trinions have been suggested recently for a unique representation and efficient analysis of color images with three components [82]. The three components of a given color image can be mapped to the three components of a trinion there

by avoiding the redundancy issue we incurred using the quaternion representation. The introduction of the trinions has stimulated useful applications in analyzing multi-component medical images (see [83] for example). It is the intent of this thesis to discuss more in detail about trinions and their applications in edge analysis of MP-MR images.

5. A Robust Edge Detection of MP-MR Brain Images

5.1. Introduction

Most approaches that are suggested in the literature for holistic processing of color images depend on the color intensity information to extract features for different applications. However, other than the intensity, color images have at least two other attributes (the hue and the saturation). For applications such as edge detection, texture analysis and pattern recognition, for example, all three information are vital. The proposed scheme in this thesis tries to address the above issues by introducing a new "truly" holistic color representation and analysis scheme based on a solid mathematical model. The method keeps the inter correlation information that is embedded across the different channels/bands of color images. The proposed method uses the three component trinions to map the three color components of a color image to a single number (trinion) and applies higher order Fourier transforms in the new space.

A trinion is defined with one real and two "imaginary" components (will be discussed more in detail in section 5.5 later). The advantage of the use of trinion is that it allows a holistic representation of color images (or three channel images in general) and the respective Fourier transforms allow their analysis as one entity without the need to separate the different bands.

Algorithm used for the edge detection scheme applied to multi-parametric MR images is comprised of the following steps:

- ✓ A first step utilizes image intensity normalization on the different MR components. A normalization of T1W and T2-FLAIR image signal intensities was necessary to correct for variations between serial scans of the same patient. Contrast limited adaptive histogram equalization was applied on the T1W and T2- FLAIR images

intensities. ADC images did not require normalization as they were already converted to absolute units during processing.

- ✓ Then the three MR sequences (in our case: T1- weighted, T2-FLAIR, and ADC) are combined as an RGB color image.
- ✓ The third step of the proposed edge detection scheme utilizes a color space transformation. Each component of RGB image is first normalized to its maximum and then the normalized RGB image is transformed to the HSL (Hue, Saturation and Luminosity) color space. The RGB to HSL conversion was needed as the later color space is believed to be closer to the human visual perception and hence is potentially helpful for the proposed edge detection scheme.
- ✓ Next, the three MR sequences, now a color in the HSL space, are mapped to a trinion. The T1W, T2- FLAIR, and the ADC parameters were mapped as the real and the two imaginary components of a trinion, in that order. Note that, in a previous study it has been shown that the order of the mapping does not affect the analysis [84].
- ✓ A voxel-by-voxel analysis is carried out by computing the Trinion Fourier Transform (to be discussed later) based on a translating localizing window of size 3×3. As this operation is done in the trinion space, there is enough number of numbers to extract meaningful statistics using such small enough localizing window. Following that, vectorial principal component analysis (PCA) was applied on each (3×3 localized) TFT transformed image, each resulting in a trinion valued output in the new PCA space each of which is a 3×3 matrix in this case. This step was needed in to reduce some redundancy in the multi-channel data. The PCA algorithm is freely available on the Algorito website at http://algorito.com/algorithm/principalcomponent-analysis-pca-transform.

- ✓ On the resulting 3×3 trinion valued matrix, a second order feature, call it F, is computed and assigned to the central voxel value.
- ✓ The above step is repeated across all voxels that are included in the selected region of interest. Once the calculation is done across all voxels, the resulting matrix is plotted as an edge map.

The next subsection of this chapter discusses the proposed method following each steps described above.

5.2. Method of MP-MR Image Acquisition

It is briefly discussed in chapter three of section 3.1.3 (Hardwar/instrumentation) how images are acquired from MRI imaging machine. Here let's summarize how images are acquired from MRI as follows: Protons and neutrons of the nucleus of an atom possess an angular momentum that is called spin. These spins cancel if the number of subatomic particles in a nucleus is even. Nuclei with an odd number exhibit a resultant spin that can be observed outside of the atom. This is the basis of magnetic resonance imaging (MRI) [86]. In MRI, spins of nuclei are aligned in an external magnetic field. A high frequency electromagnetic field then causes spin precession that depends on the density of magnetized material and on its molecular binding. The resonance of the signal continues for some time after this radio signal is switched off. The effect is measured and exploited to create an image of the distribution of the material.

5.3. Type of Data Used

The edge detection scheme discussed in this thesis has been tested on the available multi-parametric MR images from a cohort of 29 patients treated for Glioblastoma multiforme (GBM) used in the previous study in [86].

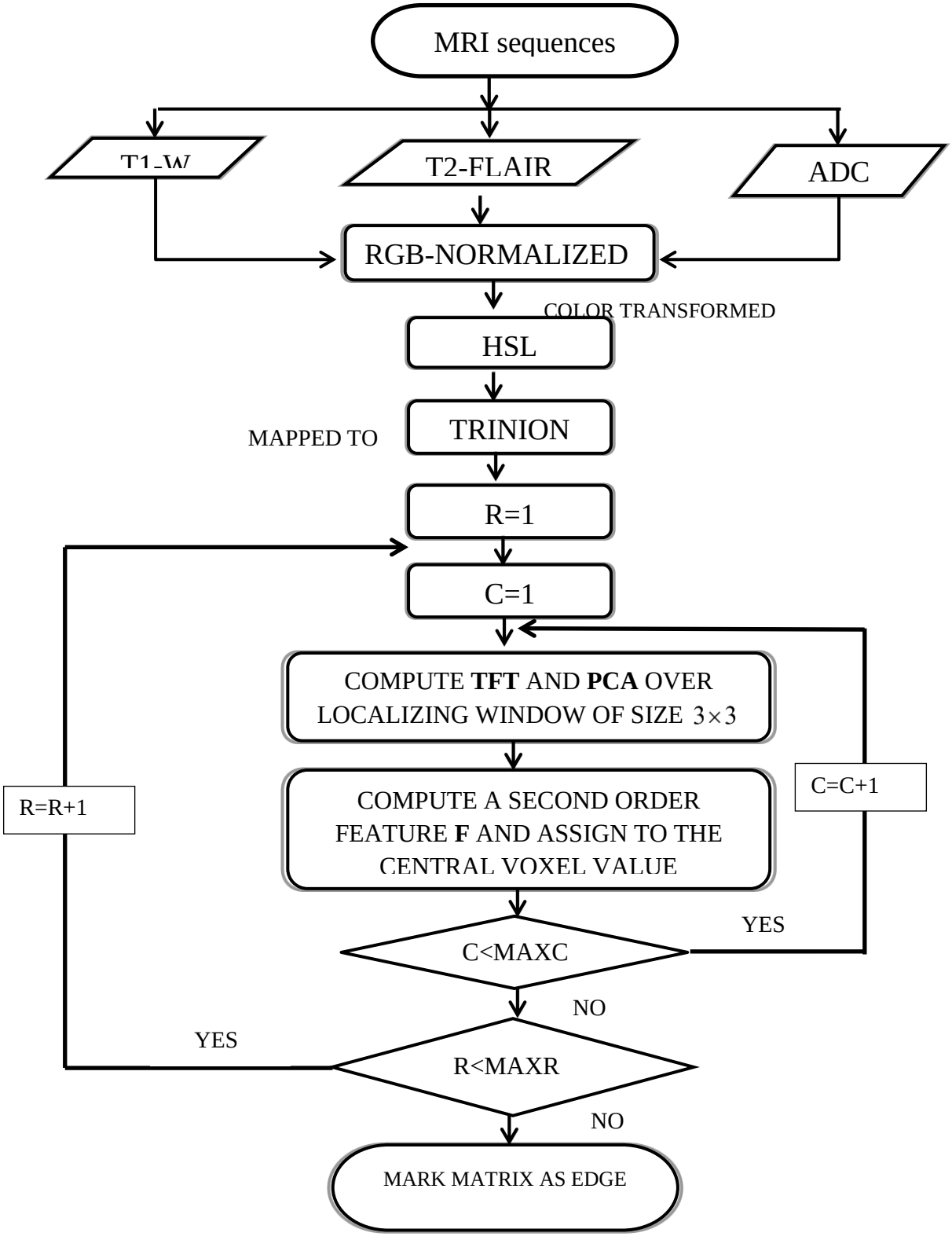

Figure 5.1: Block diagram of the proposed edge detection method.

Contrast-enhanced T1-W gradient-echo and T2-FLAIR spin-echo as well as ADC MRI of the patients acquired before-, during-, and after-radiation therapy were available for analysis.

For each patient, all serial MR volumes were registered to the orientation of the baseline T1-W image volume using the normalized mutual information algorithm and re-sampled to a common resolution using trilinear interpolation [89].

5.4. Color Space Selection and Transformation

The color perceived by a human eye can be defined as a linear combination of R, G and B. For that reason it is very reasonable to focus on RGB color spaces. Most of the discussions of color image analysis in this thesis are focused on RGB color images (also assuming the MP-MR image trios are also RGB types). As said above, an RGB color space is seen as a representation of color images in a three dimensional rectangular coordinate system. However there are other color spaces which might be more useful in applications than just RGB and transforming images from RGB space to a different coordinate system can be very beneficial. One commonly used such space is the HSL (also known as HSB or HSV) color space where H refers hue, S refers saturation and L refers luminance or lightness or intensity. This color space is believed to be most likely the kind of color perceived by our eyes. We can think of the HSL color space as a representation of an RGB color image in a cylindrical coordinate system [87]. The axis of this cylinder passes through the achromatic or grey points (R = G = B), often called the achromatic axis. So for a given RGB image in this cylindrical coordinate system, the hue (H) corresponds to the angular coordinate, the saturation (S) corresponds to the distance from the achromatic axis and the luminance (L) corresponds to the coordinate of a color on the achromatic axis. In short, an RGB color image in the RGB 3D rectangular coordinate space can be represented by a position (L), a color angle (H) and a color magnitude (S) in the HSL cylindrical coordinate space [88].

After having the right test images of MP-MRI, the next step in this edge detection scheme is, for every scan, to combine the T1W, T2- FLAIR, and the ADC images to make a RGB color image h(x, y) which can be mapped to a trinion as follows:

$$h(x,y) = R(x,y) + iG(x,y) + jB(x,y) \tag{5.1}$$

Then each component is normalized to its maximum. The (normalized) RGB image is then transformed to the HSL utilizing a color space transformation. The original RGB image was converted to HSL color using the following formula [86]:

$$H = \arctan\left(\frac{v_2}{v_1}\right), \quad S = \sqrt{{v_1}^2 + {v_2}^2}\ , \quad L = \left(\frac{R+G+B}{\sqrt{3}}\right) \tag{5.2}$$

where $v_1 = \frac{(2R-G-B)}{\sqrt{6}}$, and $v_2 = \frac{(R-G)}{\sqrt{2}}$.

The RGB to HSL conversion was needed as the later color space is believed to be closer to the human visual perception and hence is potentially helpful for our edge detection scheme.

5.5. HSL Color Image Mapping to the Trinion Space

Following the above step, the resulting color image in the HSL space is mapped to a trinion. Trinions allow a vectorial representation of color images which have recently been proposed and have shown very great promises in different applications. Due to their convenience in representation of three component color images as well as their ability to display full three dimensional color spectra, trinions are adopted as a basis for designing robust edge detection scheme for the MP-MR images in this thesis. Trinions have one real term and two imaginary components. A trinion number t is defined as:

$$t = a + ib + jc \tag{5.3}$$

where a, b and c are real numbers, i and j are operators satisfying the following multiplication rules:

$$ii = j,\ jj = -i \text{ and } ij = ji = -1 \tag{5.4}$$

The three basis elements, {1, i, j} of trinions form an abelian (commutative) group where 1 is the multiplicative identity element. Trinions are associative as well as distributive with respect to addition and multiplication [89]. As opposed to the quaternion counterpart, trinion multiplication is commutative. Any trinion number *t* can be expressed as the sum of a real part and a vector part as:

$$\mathrm{t} = \mathrm{S(t)} + \mathrm{V(t)} \tag{5.5}$$

where $S(t) = a$ is the real part and $V(t) = ib + jc$ is the vector part. It can also be written in the following form:

$$\mathrm{t} = |\mathrm{t}|(\cos\varphi + \mu\sin\varphi) \tag{5.6}$$

where $|t| = \sqrt{a^2 + b^2 + c^2}$, $\mu = \frac{V(t)}{|V(t)|}$ and $\varphi = tan^{-1}\left(\frac{|V(t)|}{S(t)}\right)$, $0 < \varphi < \pi$ are the amplitude (modulus), the eigen axis and eigen angle (phase) respectively. When $|\mathrm{t}| = 1$ it is a unit trinion and when $a=0$ it is a pure trinion. More interesting properties of trinions are discussed in the literature [89].

Two working definitions for the trinion Fourier transform (TFT) have been suggested [89]. The TFT of type I and its inverse (ITFT) are given by:

$$T1(u,v) = \int_{-\infty}^{\infty}\int_{-\infty}^{\infty} h(x,y)\,(\cos(2\pi(ux+vy)) - \mu_1 \sin(2\pi(ux+vy)))\ dxdy \tag{5.7}$$

$$h(x,y) = \int_{-\infty}^{\infty}\int_{-\infty}^{\infty} T(u,v)\,(\cos(2\pi(ux+vy)) + \mu_2 \sin(2\pi(ux+vy)))\ dudv \tag{5.8}$$

where *h(x, y)* is generally a trinion valued image function, μ_1 is a unit pure trinion, and μ_2 is a trinion such that the product $\mu_1\mu_2$ = -1. The choice of μ_1 and μ_2 is arbitrary. As done in previous studies [6], the choices of μ_1 and $\mu_2$in this thesis are given by $\mu_1 = \frac{(i-j)}{\sqrt{2}}$ and $\mu_2 = \frac{(-1-i+j)}{\sqrt{2}}$.

There exists a type II TFT and its inverse (ITFT) in the literature [89] which are given by:

$$T2(u,v) = \int_{-\infty}^{\infty}\int_{-\infty}^{\infty} h(x,y)(\cos(2\pi ux) - \mu_1 \sin(2\pi ux))(\cos(2\pi vy) - \mu_2 \sin(2\pi vy))dxdy \qquad (5.9)$$

$$h(x,y) = \int_{-\infty}^{\infty}\int_{-\infty}^{\infty} T2(u,v)(\cos(2\pi ux)) + \mu_3 \sin(2\pi ux))\cos(2\pi vy) + \mu_4 \sin(2\pi vy))dudv \qquad (5.10)$$

where μ_1, μ_2 are unit, pure trinions and, and μ_3, μ_4 are trinions satisfying $\mu_1\mu_3 = -1 = \mu_2\mu_4$ However, many operations of interest including convolutions and correlations are shown to be easier using the type I TFT than type II TFT [89], and hence the former has been adopted in the current study.

The discrete TFT of type I and its inverse are computed as follows:

$$T(u,v) = \frac{1}{MN}\sum_{x=0}^{M-1}\sum_{y=0}^{N-1} h(x,y)\left(\cos\left(2\pi\left(\frac{ux}{M} + \frac{vy}{N}\right)\right) - \mu_1 \sin\left(2\pi\left(\frac{ux}{M} + \frac{vy}{N}\right)\right)\right) \qquad (5.11)$$

$$h(x,y) = \sum_{u=0}^{M-1}\sum_{v=0}^{N-1} T(u,v)\left(\cos\left(2\pi\left(\frac{ux}{M} + \frac{vy}{N}\right)\right) + \mu_2 \sin\left(2\pi\left(\frac{ux}{M} + \frac{vy}{N}\right)\right)\right) \qquad (5.12)$$

where $M \times N$ is the total number of voxels (pixels) present in the selected region of interest (window) of the original image, u=0, 1… N-1 and v=0, 1… M-1, are the discrete frequencies along the horizontal and vertical directions respectively.

The converted RGB color brain MP-MR image is mapped to a trinion as $h(x,y) = H + iS + jV$ in HSV color space. It has already been shown previously that the order of the mapping to a trinion doesn't affect the image analysis [89].

5.6. Edge Detection in the Trinion Space

Following the above step, a voxel by- voxel analysis is carried out by computing the TFT, based on a translating localizing window of size 3×3. On the resulting 3×3 trinion valued matrix, a second order feature was computed and assigned to the central voxel value. For the purpose of edge detection, the following feature F was computed [90]:

$$F = Metric\left(\frac{\log(1+p(x,y))}{\log\left(1+\max\limits_{x,y}\{p(x,y)\}\right)} \right) \tag{5.13}$$

where $p(x,y)$ is the square amplitude ('power') of the TFT, and Metric is a second order statistical feature (variance, standard deviation, sum-mean, cluster shade, cluster prominence, etc.). The above step is repeated across all voxels that are included in the selected region of interest (note that the scheme is applied on the whole image in this work without the need for selecting a region of interest). Once the calculation is done across all voxles, the resulting matrix is plotted as an edge map. The formulas used for computing the second order features are exactly the ones used by Haralick [90]. However, the probability distribution functions are not computed through calculation of gray level co-occurrence matric (GLCM) as Haralick did but are computed from the local calculations of the trinion Fourier transform.

6. Results and Discussion

6.1. Experimental Results

6.1.1. First Order Gradient and Second Order Laplacian Based Edge Detection Approaches Applied on MP-MRIs

Presumably useful (dominant) edges in this case include the brain and other important structures including the vents, the tumor and surrounding edema. In this case, the tumor is seen surrounded by edema on the MP-MRI with enhanced contrast with proximity to the vent structure. None of the classical approaches were able to detect the useful edges successfully.

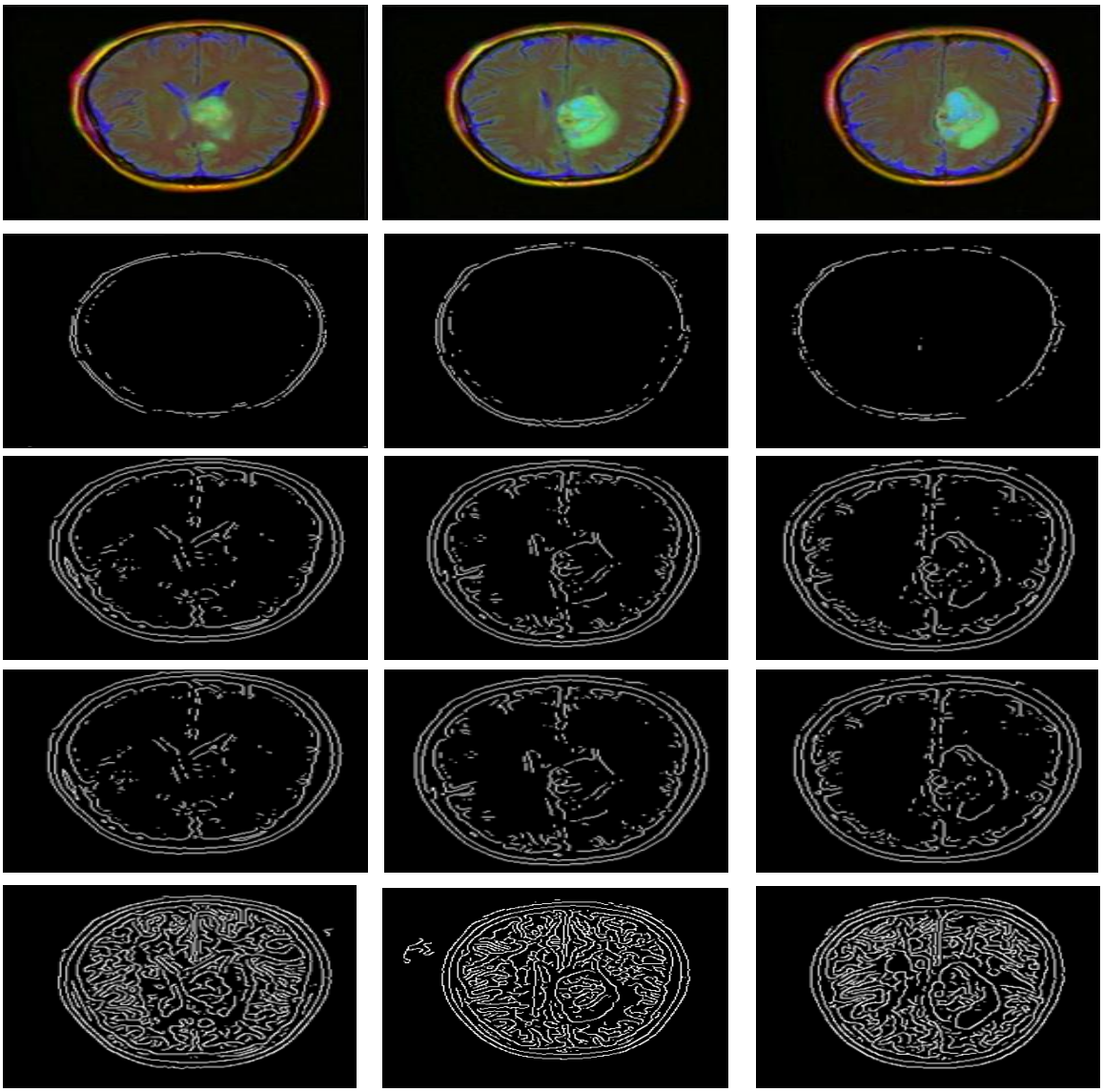

Figure 6.1: First order gradient and second order Laplacian based edge detection approaches applied on MP-MRI: T1, T2-FLAIR and ADC combined color images (row 1), Sobel edge map (row 2), LOG edge map (row 3), zero-cross edge map (row 4) and Canny edge map (row 5).

6.1.2. Vectorial approaches: The max gradient approach and the proposed method

Among different vectorial edge detection approaches available in literatures, the max gradient method (the max gradient implementation used in this thesis was based on a recent version of the algorithm by J. Henriques which is freely available from the Matlab Central website). Like the trinions, quaternions and other vectorial approaches, the max gradient method treats a RGB color image as a three dimensional vector. The edge detection results found using the max gradient method were not satisfactory for MP-MRIs. Here what is needed is to show with demonstrating examples that the trinion formulation and analysis is much more powerful than standard vectorial approaches. The examples in Fig. 6.2 show cases where the max gradient methods fail to detect edges appropriately.

The above results clearly indicate that an effective color edge detection requires not just a vectorial scheme but a more systematic manipulation of the inter correlation information that is embedded among the monochromes (vector components) that make up the color image.

Note that as the results computed in the quaternion space are very similar to those computed in the trinion space (the proposed algorithm), results computed in the quaternion space are intentionally omitted from the results presented in this thesis.

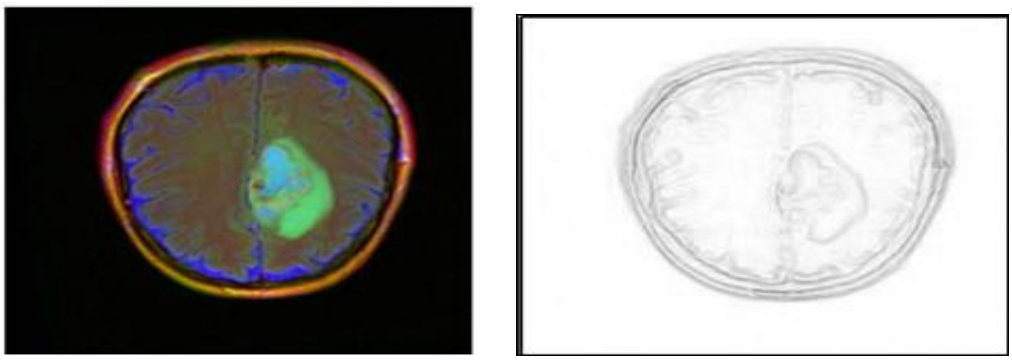

Figure 6.2: vectorial max gradient approach applied on MP-MRI: T1, T2-FLAIR and ADC combined color images (left), max gradient edge map (right) .

6.1.3. Testing the proposed approach on MP-MRIs

The experimental results presented in this study are qualitative mainly relating edge detection of tumor and other important regions of brain MRI using the proposed edge detection tool with that of manual delineations by experts. Two main issues have to be considered when applying the proposed algorithm in edge detection of the MP-MRI data sets. Primarily the proposed scheme assumes that the different MR images (parameters) behave well so that the color assumption and representation of the MP-MRI is acceptable. For example, not all glioma tumors show elevated ADCs. This can create inconsistency, for example, when trying to detect tumor edges. Hence such cases should be excluded from the analysis. This issue of course is not present in actual color images (the test images for example). Another issue is possible registration inaccuracy, which in most cases is unavoidable, accompanied by the fact that it has been also applied interpolation as a preprocessing step so that all MR image parameters assume a common resolution. These could potentially pose a challenge in implementing the proposed edge detection scheme. Figure 6.3 presents the edge detection results found using the proposed algorithm applied on representative MP-MRI slices. All the three axial slices are confirmed to contain no tumor or any other lesion in them. As can be seen on the generated edge map, the brain tissue is well segmented with some difficulties around skull boundaries which may have resulted from some image registration inaccuracies. Structures such as the vent were also effectively detected.

Figure 6.4 presents three chosen MRI slices of patients diagnosed with GBM. The red contours on the combined color image (combined T1-W, T2- FLAIR, and ADC) show the GBM tumors as delineated by a radiation oncologist which were done based on contrast enhancement identified on the T1-W images. The algorithm performs well in detecting the tumor edges, which is one of the most difficult tasks in edge detection of the MP-MRIs. That was (qualitatively) in a very good agreement with the ground truth information which is the

oncologist's contour drawn in red. There appeared other edges detected within the tumor boundaries showing tumor heterogeneity which could be a useful finding. Other structures such as the brain, vent and the skull boundary were also satisfactorily detected.

The examples in Fig.6.5 and Fig. 6.6 were composed of slices taken from GBM patients where the tumors appeared surrounded by a pronounced amount of edema (mostly identified on the T2-FLAIR and sometimes on the ADC also). This is quite a challenging task. The generated edge maps tend to cover more area outside the respective contours by the expert physician. Such differences are expected between the manual contours and that of the edge maps. As opposed to relying only on a single MRI parameter for manual tumor region delineation, the purposed scheme tries to automate the process making use of the combined multiple MR parameters to generate the edge maps using a suitable mathematical setup. The first slice in Fig. 6.6 shows that the proposed method is capable of identifying the edges of even very small tumors. As can be seen on the edge maps, it is obvious that further thresholding might be needed to differentiate the tumor from the surrounding edema. Such a threshold should essentially be adaptive while finding such an adaptive thresholding scheme is beyond the scope of this thesis project work.

Note that the edge detection scheme proposed in this work is developed mainly for use in tissue edge detection of the brain focusing on tumor (disease) edge detection. For the results presented in this study, however, we applied the algorithm to the whole image slice including the skull boundary. Also, for the trinion implementation of the proposed algorithm, use of the Fast Fourier Transform (FFT) to calculate the respective TFTs allows very fast computation even when applied on the whole image slice. As the edge map generation involves a local analysis, inclusion of non-tissue structures, such as the skull and its boundaries, and other structures such as the eye, should not affect the analysis considerably. However, it should be

mentioned that in most image processing applications involving MRIs, mostly the skull is taken off before further analysis is carried out.

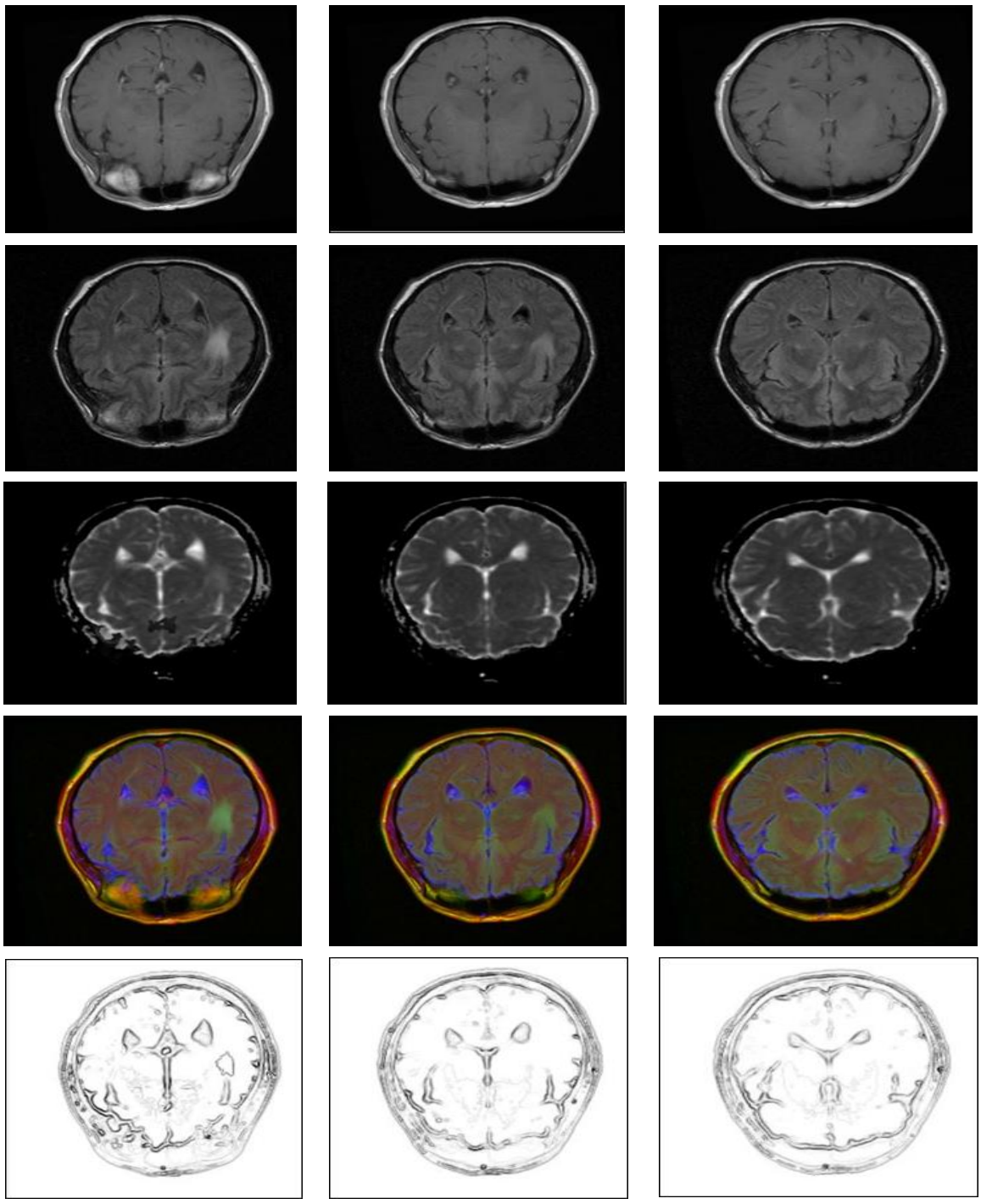

Figure 6.3: Row 1 to 3 is original T1, T2-FLAIR and ADC images respectively of different slices of the same patient: row 4 contains the respective combined color images and row 5 contains corresponding edge maps generated in the trinion space.

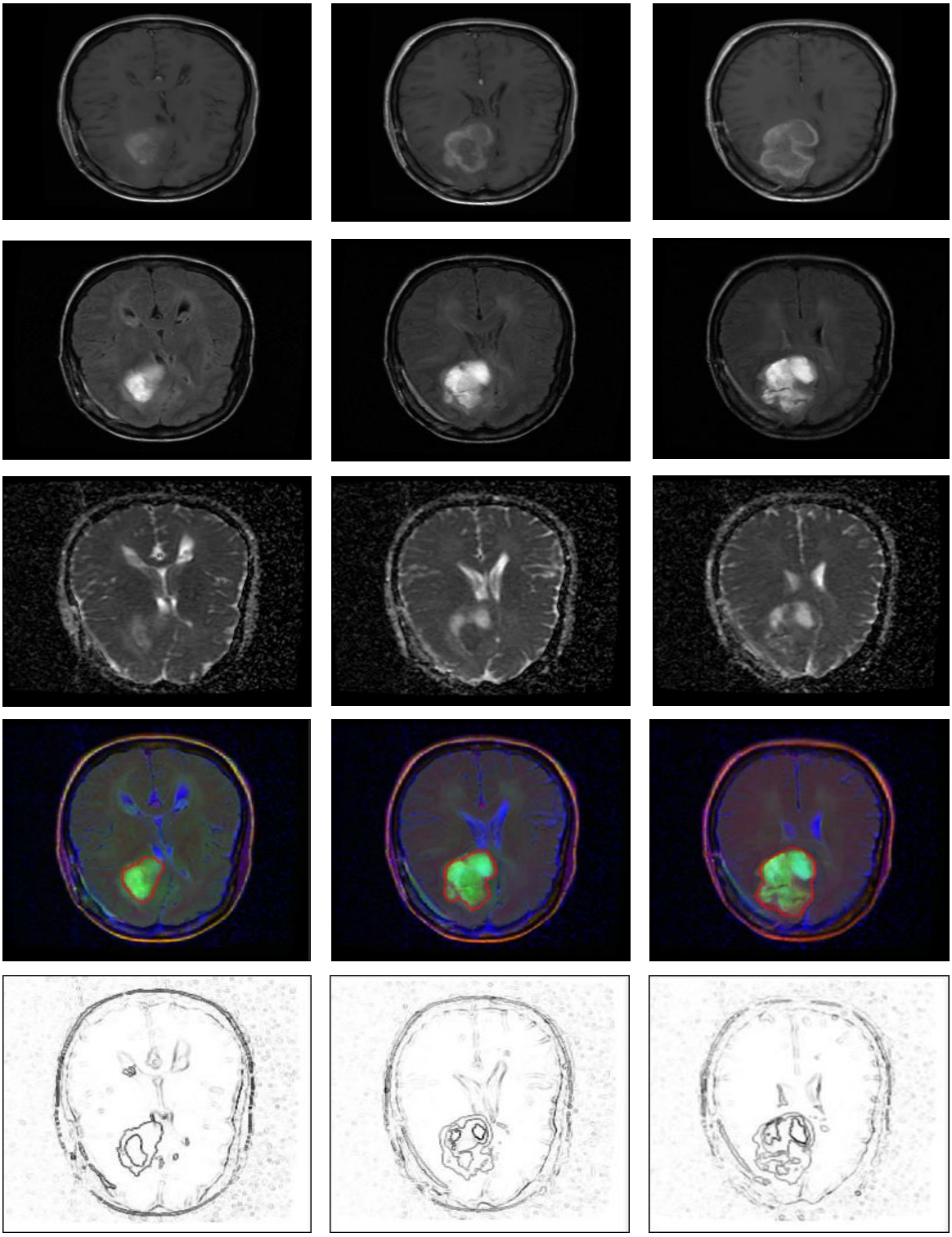

Figure 6.4: Row 1 to 3 are original T1, T2-FLAIR and ADC images respectively of different slices of the same patient containing contrast enhanced glioma tumors; row 4 contains the respective combined color images (red contour shows tumor delineations by a radiation oncologist) and row 5 contains the corresponding edge maps generated in the trinion space.

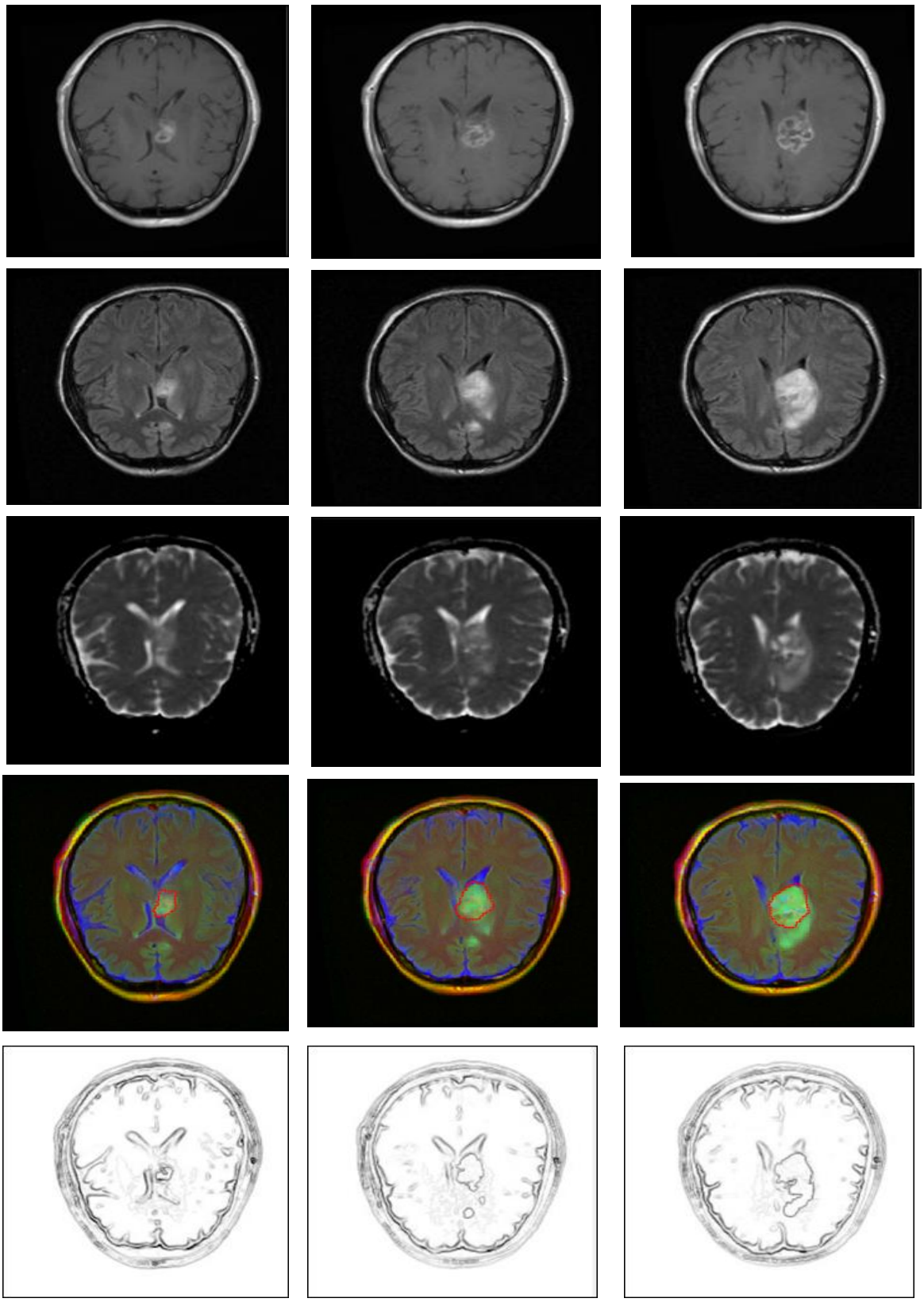

Figure 6.5: Row 1 to 3 are original T1, T2-FLAIR and ADC images respectively of different slices of the same patient containing contrast enhanced glioma tumors; row 4 contains the respective combined color images (red contour shows tumor delineations by a radiation oncologist) and row 5 contains the corresponding edge maps generated in the trinion space.

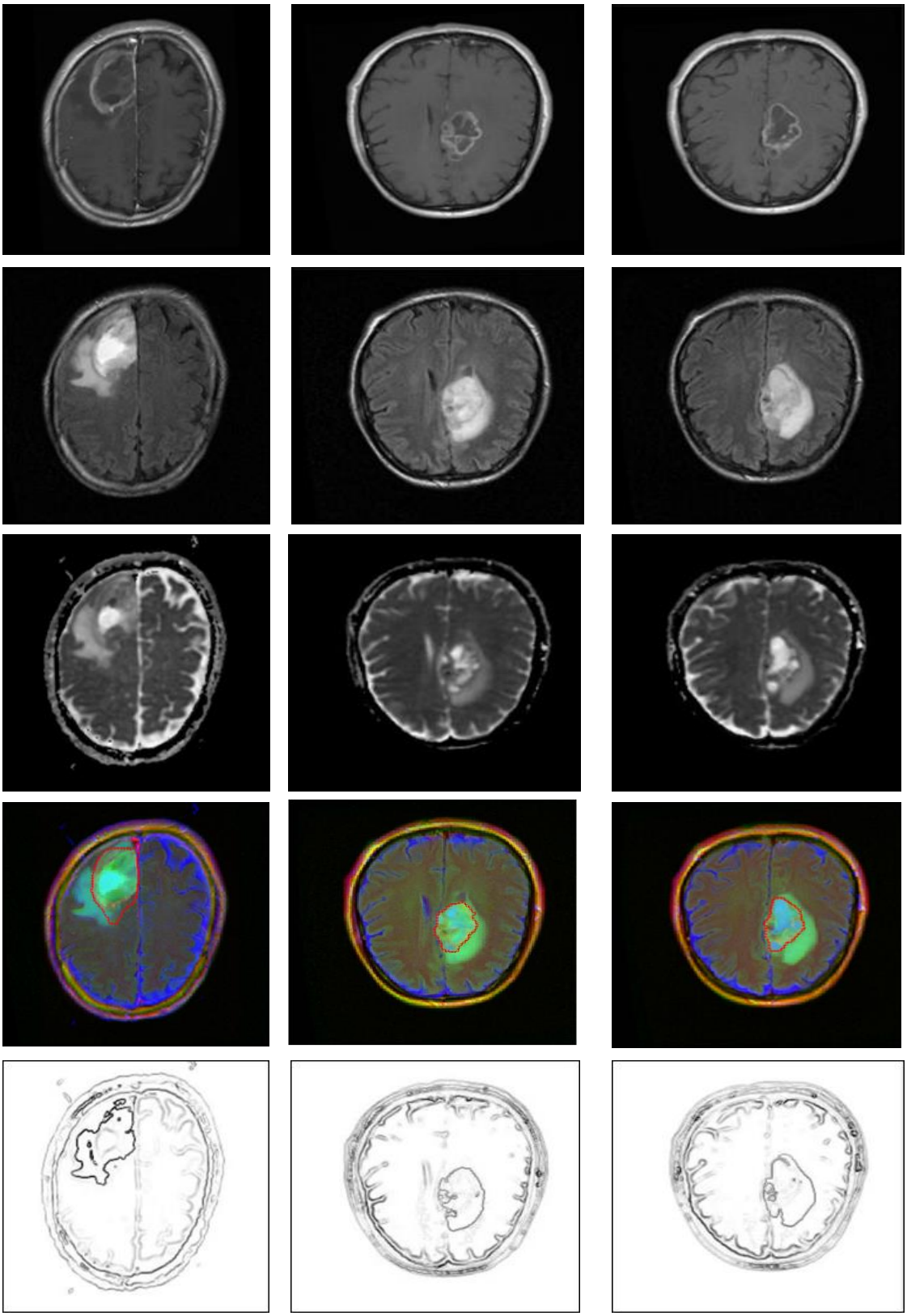

Figure 6.6: Row 1 to 3 are original T1, T2-FLAIR and ADC images respectively of different slices of two patients containing contrast enhanced glioma tumors; row 4 contains the respective combined color images (red contour shows tumor delineations by a radiation oncologist) and row 5 contains the corresponding edge maps generated in the trinion space.

7. Conclusion and Recommendations

7.1. Conclusion

In this thesis work a promising approach has been proposed for use in edge detection of color images. Major interest of the work was development of an edge detection tool that can be used in analyzing edges of multi parametric MR images. The proposed method uses a holistic representation of the color images in three (trinion) space and applies trinion based Fourier transforms to generate edge maps. The multiple parameters of the MR scans were assumed to be color channels/bands. Prior to developing the proposed image processing tool, fundamentals of medical imaging techniques and modalities have been discussed thoroughly focusing on MRI. MRI architectures, principles, and image acquisition processes are described. The principles of multi parametric MR imaging are discussed and their advantages are reviewed. Different edge detection approaches already available in the literature have been discussed and assessed. Generally two groups of techniques exist in these regard: serial and vectorial. The former requires separation of color components for analysis while the vectorial approaches are holistic. Holistic representation of color pixels is the major building block of the proposed scheme in this thesis project. The main reason to opt for holistic approaches is the fact that the multiple components of a color image are essentially correlated to each other and such correlation information is believed to be vital for many image processing applications one of them being feature based edge detection. The scheme applies recent mathematical theory of trinions and Fourier transforms defined in the trinion space for effective image statistical feature extraction of color images. These features were computed locally on the images under consideration. It was these features that were used to generate the required edge maps. In this regard, the thesis also discussed various vectorial approaches which are already available in the literature.

The various tests performed on the multi parametric MR images taken from patients treated for the highest grade glioma tumors known by the name Glioblastoma Multiforme clearly showed that the trinion formulation is a very useful edge detection tool. Like many other vectorial approaches, the proposed scheme is holistic in the sense that it takes into account the inter-correlation information that is embedded within color components. But it is also highly more effective and efficient than most other vectorial approaches such as the max gradient operator which resulted mainly from a more systematic manipulation of the vector components.

7.2. Recommendation

Only medical data (multi parametric MR images) used in previous research works has been used to assess the effectiveness of the proposed scheme. Though good amount of data is already available in local hospitals and clinics, none of them were found fit for the current research. Primarily the local data were not taken from a cohort and hence had no patients findings or ground truth information with them. Such information was vital for the current research.

All computations ware done using a Matlab (version 14) platform on a core I7 laptop. Typical processing times for a 256x256 color image until an edge map is populated is around 20 seconds, which could be considered fast. The trinion Fourier transforms was computed by a repeated use of the Fast Fourier Transform (FFT). The code could be optimized so that it could run much faster while no effort has been exerted to do that in this thesis. However, if the scheme has to run in real time, high performance computing could be a good option. This is vital in particular when the input color image is of larger size.

7.3. Future works

There are still rooms to improve the performance of this edge detection scheme particularly as the color image under consideration gets more complex. After computing the windowed Fourier transforms, ways to extract even more powerful features than the once used in this study (second order variance, standard deviation, etc.) can be beneficial. This for example can mean searching for statistical features which are less sensitive to subtle changes within the color image such as noise. Furthermore, two relaxation (T1 and T2) and one functional (ADC) MR parameters are used in this study. Looking at just one set at a time, i.e. three relaxation or three functional parameters, can be an interesting test to try at least for the sake of comparison. Resolving these and similar other issues is pending further investigations. A further investigation to be able to compute more powerful and less sensitive (towards subtle changes within the color image under consideration) TFT based features can be beneficial to improve the performance of the proposed edge detection algorithm. In principle, other than MRIs, the proposed scheme can also be applied to images acquired through other modalities such as CT, PET, and the like. The thesis also lacks rigorous validation work which could require an observer study. Also investigation of clinical implications of the results awaits further research.

References

1. M. Sonka, V. Hlavac, R. Boyle, Image Processing Analysis and Machine Vision, second ed., Thomson Asia Pte Ltd and PPTPH, Berlin, 2001.
2. J. Canny, A computational approach to edge detection, IEEE Trans. Pattern Anal. Mach. Intell., 8(6). Pp.679-698, 1986.
3. P. E. Trahanias, A. N. Venetsanopoulos, Color edge detection using vector order statistics, IEEE trans. Image Proc., 2(2), pp. 259-264 1993.
4. H. Tang, E. X. Wu, Q. Y. Ma, D. Gallagher, G. M. Perera, T. Zhuang, MRI brain image segmentation by multi-resolution edge detection and region selection, Computerized Medical Imaging and Graphics, vol. 24, pp. 349-357, 2000.
5. R. Lukac, B. Smolka, K. Martin, K. N. Plataniotis, A. N. Venetsanopoulo, Vector Filtering for Color Imaging: Opening a world of possibilities, IEEE Signal Proc. Magazine, 22(1), pp. 74–86, Jan. 2005.
6. S.-Y. Zhu, A. N. Venetsanopoulos, K. N. Plataniotis, Comprehensive analysis of edge detection in color image processing, Opt. Eng., 38(4), pp. 612–625, Apr. 1999.
7. T.A. Ell and S.J. Sangwine, Hyper complex Fourier transforms of color images, IEEE Transactions on Image Processing, 16(1), 22–35 2007.
8. Dawit Assefa, L. Mansinha, K. F. Tiampo, H. Rasmussen, K. Abdella, The trinion Fourier transform of color images, Signal Processing, vol. 91, pp. 1887–1900, 2011.
9. Dawit Assefa, H. Keller, D. A. Jaffray, Multiparametric MR image processing using higher dimensional vector algebra, ACTA Press, Proceedings of the IASTED International Symposia on Imaging and Signal Processing in Healthcare and Technology (ISPHT' 11), Washington, DC, USA, May 2011.
10. Dawit Assefa, H. Keller, D. A. Jaffray, Signal Analysis of Multi-Parametric MR Images in Higher Order Fourier Spaces, International Journal of Computational Bioscience, Vol. 4, No.1, 2013.
11. M. A. Oskoei, H. Hu, A survey on edge detection methods,Technical report: CES-506,United Kinkdom,29 February 2010.
12. E. Trucco, A. Verri, Introductory Techniques for 3-D Computer Vision, Prentice Hall, 1998.
13. R. M. Kumar, R. Saxena, Algorithm and technique on various edge detection: a survey, Int. J. (SPPIJ) , Vol. 4, No.3, June 2013.

14. S. Jansi, P. Subashini, Optimazed adaptive thresholding based edge detection method for MRI brain images; Int. J. Comp. App (0975-8887), Vol.20, August 2012.
15. A. Mittal, S. Sofat, E. Hancock, Detection of edges in color images: A review and comparisonof state of the art techniques, M. Kamel, F. Karray, and H. Hagras (Eds.): AIS 2012, LNCS 7326, pp. 2500-259, 2012.
16. S. Zhu, K. N. Plataniotis, A. N. Venetsanopoulos, Comprehensive analysis of edge detection in color images processing,Optical Engineering, Vol. 38, No. 4, April 1999.
17. M. Basu, Gaussian-Based Edge-Detection Methods - A Survey, IEEE Transactions on Systems, Man, and Cybernetics—Part C: Applications and Reviews, Vol. 32, No. 3, pp. 252-260, August 2002,.
18. S. Lu, Z. Wang, J. Shen, Neuro-fuzzy synergism to the intelligent system for edge detection and enhancement, Journal of Pattern Recognition, 36 pp. 2395-2409, 2003.
19. J. Canny, A Computational Approach to Edge Detection, IEEE Transaction on Pattern Analysis and Machine intelligence, No. 6, pp. 679-698, 1986.
20. D. Heric, D. Zazula, Combined edge detection using wavelet transform and signal registration, Journal of Image and Vision Computing, 25, pp. 652-662, 2007.
21. M. Y. Shih, D. C. Tseng, A wavelet based multi resolution edge detection and tracking, Journal of Image and Vision Computing, 23 , pp. 441–451, 2005.
22. Y. Yu, C. Chang, A new edge detection approach based on image context analysis, Journal of Image and Vision Computing, 24, pp. 1090–1102, 2006.
23. S. Konishi, A. L. Yuille, J. M. Coughlan, S. C. Zhu, Statistical Edge Detection: Learning and Evaluating Edge Cues, IEEE Transactions on Pattern Analysis and Machine Intelligence, Vol. 25, No. 1, pp. 57-74, 2003.
24. J. Wu, Z. Yin, Y. Xiong, The Fast Multilevel Fuzzy Edge Detection of Blurry Images, IEEE Signal Processing Letters, Vol. 14, No. 5, pp. 344-347, 2007.
25. D. Marr, E. Hildreth, Theory of edge detection, Proc. Royal Society of London, B, 207, pp. 187–217, 1980,.
26. R. Kasturi, R. C. Jain, Eds. Computer vision: principles, IEEE Computer Society Press, Los Alamitos, CA, 1991.
27. B. G. Schunck, Edge detection with Gaussian filters at multiple scales, in Proc. IEEE Comp. Soc. Work. Comp. Vis., pp. 208–210 1987.
28. A. P.Witkin, Scale-space filtering, in Proc. Int. Joint. Conf. Artificial Intelligence, Vol. 2, 1983, pp. 1019–1022.

29. F. Bergholm, Edge focusing, IEEE Trans. Pattern Anal. Machine Intell, Vol. PAMI-9, pp. 726–741, June 1987.
30. V. Lacroix, The primary raster: A multi resolution image description, in Proc. 10th Int. Conf. Pattern Recognition, 1990, pp. 903–907.
31. D. J. Williams, M. Shah, Edge contours using multiple scales, Comput. Vis. Graph Image Process, Vol. 51, pp. 256–274, 1990.
32. G. Deng, L. W. Cahill, An adaptive Gaussian filters for noise reduction and edge detection, in Proc. IEEE Nucl. Sci. Symp. Med. Im. Conf., 1994, pp. 1615–1619.
33. M. Bennamoun, B. Boashash, J. Koo, Optimal parameters for edge detection, in Proc. IEEE Int. Conf. SMC, Vol. 2, pp. 1482–1488, 1995.
34. P. Perona, J. Malik, Scale-space and edge detection using anisotropic diffusion, IEEE Trans. Pattern Anal. Machine Intell, Vol. 12, pp. 629–639, July 1990.
35. R. M. Haralick, Ridge and Valley on Digital Images, Computer Vision, Graphics and Image Processing, 22, 28-38, 1983.
36. G. Giraudon, Edge Detection from Local Negative Maximum of Second Derivative, in Proceedings of IEEE, International Conference on Computer Vision and Pattern Recognition, 643-645, 1985.
37. D. Ziou, Line Detection Using an Optimal IIR Filter, Pattern Recognition, 24(6), 465-478,1991.
38. K. Koundinya, B. Chanda, Detecting Lines in Gray Level Images Using Search Techniques, Signal Processing, 37, 287-299, 1994.
39. X. Chen, H. Chen, A novel color edge detection algorithm in RGB color space, Proc. of IEEE 10th International conference on signal processing, 793-796, 2010.
40. M. A. Ruzon, C. Tomasi, Edge, Junction, and Corner Detection using Color distributions, IEEE Transactions on Pattern Analysis and Machine Intelligence, 23, no. 11, Nov. 2001.
41. R. Nevati, A Color edge detector and its use in scene segmentation, IEEE Transactions on Systems, Man and Cybernetics, SMC-7, No. 11, Nov. 1977.
42. Shiozaki, Edge extraction using entropy operator, Computer Vision, Graphics, and Image Processing, Vol. 36, No. 1, 1-9, Oct. 1986.
43. M. Hedley, H. Yan, Segmentation of Color images using spatial and color space information, Journal of Electronic Imaging, 374-380, 1992.
44. T. Carron, P. Lambert, Color edge detection using jointly hue, saturation and intensity, Proc. of IEEE International Conference on Image Processing, 977-981, 1994.

45. J. Fan, W. G Aref, M. S Hacid, A. k Elmagarmid, An improved automatic isotropic col-or edge detection technique, Pattern Recognition Letters, 22, 1419-1429, 2001.
46. L. Niu, W. Li, Color edge detection based on direction information measure, 6th World Cong. on Int. Cont. and Automation, 9533-9536, 2006.
47. G. Robinson, Color Edge detection, Optical Eng., 16, No. 5, 479-484, Sept. 1977.
48. S.D. Zenzo, A note on gradient of a multi-image, Computer Vision, Graphics, and Image Processing, 33, No. 1, 116-125, Jan. 1986.
49. A. Cumani, Edge detection in Multispectral Images, CVGIP: Graphical Models and Image Processing, 53, No. 1, 40-51, Jan. 1991.
50. A. Drewniok, Multispectral Edge Detection- Some Experiments on data from Landsat-TM, International J. Remote Sensing, 15,No. 18, 3743-3766, 1994.
51. M. Chapron, A chromatic contour detector based on abrupt change techniques, Proc. of International conference on Image Processing, 18-21, 3, 1997.
52. S. Dutta, B. B. Chaudhari, A Color edge detection algorithm in RGB color space, Proc. of International Conference on Advances in Recent technologies in Communication and Computing, 337-340, 2009.
53. W. Alshatti and P. Lambert, Using eigenvectors of a vector field for deriving a second directional derivative operator for color images, in Proc. 5th Int. Conf. CAIP'93, pp. 149-156, 1993.
54. A. Mittal, S. Sofa and E. Hancock, Detection of edges in Color Images: A review and evaluative comparison of state-of-the-art techniques, Springer, pp. 2-5, 2012.
55. B. Hamre, Three-dimensional image registration of magnetic resonance (MRI) head volumes, MSc Dissertation, University of Bergen, Norway, 1998.
56. A. Malaih, Brain MRI, 2012.
57. B. Turkbey, A. M. Brown, S. Sankineni, B. J. Wood, P. A. Pinto, P. L. Choyke, Multiparametric Prostate Magnetic Resonance Imaging in the Evaluation of Prostate Cancer, CA Cancer J Clin., 2015.
58. N. B. Delongchamps, M. Rouanne, T. Flam, F. Beuvon, M. Liberatore, M. Zerbib and F. Cornud, Multiparametric magnetic resonance imaging for the detection and localization of prostate cancer combination of T2-weighted, dynamic contrast –enhanced and diffusion-weighted imaging, BJU international, 2010.
59. M. P. Braeuning and E. D. Pisano, New Modalities in Breast Imaging: Digital Mammography and Magnetic Resonance Imaging. Breast Cancer Res Treat 35, 31-38 1995.

60. G. M. Kacl, P .Liu, J. F. Debatin, E. Garzoli, R. F. Caduff, and G. P. Krestin, Detection of Breast Cancer with Conventional Mammography and Contrast-enhanced MR Imaging. Eur. Radiol. 8, 194-200, 1998.
61. S. A. Feig, Decreased Breast Cancer Mortality through Mammographic Screening: Results of Clinical Trials, Radiology 167, 659-665 1988.
62. U. Fischer, L. Kopka, and E. Grabbe, Breast Carcinoma: Effect of Preoperative Contrast-enhanced MR Imaging on the Therapeutic Approach, Radiology 213, 881-88, 1999.
63. R. Verma, E. I. Zacharaki, Y. Ov, H. Cai, S. Chawla, S. Lee, E. R. Melhem, R. Wolf, and C. Davalzikas, Multi-parametric tissue characterization of brain neoplasms and their recurrence using pattern classification of MR images, Acad. Radiol, 15(8): 966-977.
64. D. Assefa, H. Keller, and D. A. Jaffray, Signal Analysis of Multi-parametric MR images in higher order Fourier Spaces, International Journal of Computational Bioscience, Vol. 4, No.1, 2013.
65. R. Gold, C. Linington, H. Lassmann, Understanding pathogenesis and therapy of multiple sclerosis via animal models: 70 years of merits and culprits in experimental autoimmune encephalomyelitis research, Brain 2006; 129:1953-71.
66. R. Hohlfeld, H. Wekerle, Autoimmune concepts of multiple sclerosis as a basis for selective immunotherapy: from pipe dreams to (therapeutic) pipelines. Proc. Natl. Acad. Sci. USA 2004; 101 (Suppl 2):14, 599-606.
67.. O Sullivan, Physical Rehabilitation, p.711-712. F.A. D. Philadelphia. ISBN 0-8036-1247-8 Head and Facial Trauma. Mosby, 2007.
68. The Internet Stroke Center. Stroke syndromes: Middle cerebral artery - inferior division. (2016, May 13). [Online] Available: http://www.strokecenter.org/prof/syndromes/syndromePage6.htm.
69. Y. R. Yadav, G. Mukerji, R. Shenoy, A. Basoor, G. Jain, A. Nelson. Endoscopic management of hypertensive intraventricular hemorrhage with obstructive hydrocephalus, BMC Neurol., 7:1, 2007.
70. M. J. Sanders and K. McKenna, Head and Facial Trauma, Mosby's Paramedic Textbook, 2nd revised Ed., Chapter 22, Mosby, 2001.
71. T. M. Deserno, Fundamentals of Biomedical Image Processing, Springer-Verlag Berlin Heidelberg 2011.
72. R. C. Gonzalez, R. E. Woods, Digital Image Processing, Pearson Education, 3rd Edition, 2002.

73. G. Waldman, Introduction to Light: The Physics of Light, Vision, and Color. Mineola: Dover Publications, 2002
74. E. H. Chudler, (2013). The retina, Retrieved February 3, 2014, from Neuroscience for Kids: http://faculty.washington.edu/chudler/retina.htm.
75. G. Wyszecki, W. S. Stiles, Color Science, Concepts and Methods, Quantitative Data and Formulas. John Wiley, N.Y., 2nd Edition, 1982.
76. J. Gomes, L. Velho, Image Processing for Computer Graphics. Springer Verlag, New York, 1997. Available: http://www.springer_ny.com/catalog/_np/mar97np/DATA/0-387-94854 6.html.
77. J. M. G. Lammens, A Computational Model for Color Perception and Color Naming, PhD Dissertation, State University of New York at Buffalo, Buffalo, New York, 1994.
78. D. Pham, C. Xu, and J. L. Prince, Current methods in medical image segmentation, Annu. Rev. Biomed Eng., Vol. 2, pp. 315-337, 2000.
79. M. Vasantha, V. S. Bharathiah, R. Dhamodhara, Medical Image Feature Extraction, Selection and Classification, Int. Jour. Eng. Sci. Tech, 2(6), pp. 2071-2076, 2010.
80. Hanbury A., The Taming of the Hue, Saturation and Brightness Color Space Proc. of the CVWW'02, Bad Aussee, Austria, 2002.
81. D. Assefa, The 1D and 2D Localized Hartley Transforms their Parallel Implementation and Applications; Color Image Analysis Using Quaternions and Trinions, PhD. dissertation, University of Western Ontario, London, Ontario, 2007.
82. D. Assefa, L. Mansinha, K. F. Tiampo, H. Rasmussen, and K. Abdella, Local quaternion Fourier transform and color image texture analysis, Signal Processing, 90(11), pp. 1825-1835, 2010.
83. D. Assefa, L. Mansinha, K. F. Tiampo, H. Rasmussen, and K. Abdella, The trinion Fourier transform of color images, Signal Processing, 91(8), pp. 1887-1900, 2011.
84. D. Assefa, L. Mansinha, K. F. Tiampo, H. Rasmussen, and K. Abdella, The trinion Fourier transform of color images, Signal Processing, 91(8), pp. 1887-1900, 2011.
85. K. D. Toennies, *Guide to Medical Image Analysis*, Advances in Computer Vision and Pattern Recognition, DOI 10.1007/978-1-4471-2751-2_2, Springer-Verlag London Limited, 2012.
86. D. Assefa, H. Keller, and D. A. Jaffray, Multi-parametric MR image processing using higher dimensional vector algebra, ISPHT, Washington, DC, USA, pp. 24-31, 2011.

87. A. Hanbury, The Taming of the Hue, Saturation and Brightness Color Space, Proc. of the CVWW'02, Bad Aussee, Austria, 2002.
88. D. Assefa, The 1D and 2D Localized Hartley Transforms their Parallel Implementation and Applications; Color Image Analysis Using Quaternions and Trinions, Phd. dissertation, University of Western Ontario, London, Ontario, 2007.
89. D. Assefa, L. Mansinha, K. F. Tiampo, H. Rasmussen, and K. Abdella, The trinion Fourier transform of color images, Sig Proc., 91(8), pp. 1887-1900, 2011.
90. R. M. Haralick, Texture Features for image classification, IEEE Transactions on systems, Man and Cybernetics, Vol. SMC-3, No. 6, November 1973.

Appendices

Trinion based technique

```
clear all
close all
clc

s_num =19;

R_comp_temp = analyze75read('P18_T1.img');
R_comp = (R_comp_temp(:,:,s_num));
w(:,:,1) = R_comp;
figure
imshow(R_comp_temp(:,:,s_num),[])

G_comp_temp = analyze75read('P18_T2.img');
G_comp = (G_comp_temp(:,:,s_num));
w(:,:,2) = G_comp;
figure
imshow(G_comp_temp(:,:,s_num),[])

B_comp_temp = analyze75read('P18_ADC.img');
B_comp = (B_comp_temp(:,:,s_num));
w(:,:,3) = B_comp;
figure
imshow(B_comp_temp(:,:,s_num),[])

tic

T_R = w(:,:,1);
T_G = w(:,:,2);
T_B = w(:,:,3);
```

```
w(:,:,1) = T_R;
w(:,:,2) = T_G;
w(:,:,3) = T_B;



w_old = w;

figure, imshow((w_old(:,:,1)),[])
figure, imshow((w_old(:,:,2)),[])
figure, imshow((w_old(:,:,3)),[])
figure, imshow(uint8(w),[])

w(:,:,1) = w_old(:,:,1);
w(:,:,2) = w_old(:,:,2);
w(:,:,3) = w_old(:,:,3);

w(:,:,1) = adapthisteq(w(:,:,1));
w(:,:,2) = adapthisteq(w(:,:,2));
w(:,:,3) = adapthisteq(w(:,:,3));


w = double(w);

w(:,:,1) = w(:,:,1)./max(max(abs(w(:,:,1))));
w(:,:,2) = w(:,:,2)./max(max(abs(w(:,:,2))));
w(:,:,3) = w(:,:,3)./max(max(abs(w(:,:,3))));

HHH = w(:,:,1);
SSS = w(:,:,2);
LLL = w(:,:,3);
FL = (HHH+SSS+LLL)/sqrt(3.0);
V_1 = (2.0*LLL-HHH-SSS)/sqrt(6.0);
V_2 = (HHH-SSS)/sqrt(2.0);
si = size(V_1);
FS = sqrt(V_1.^2+V_2.^2);
FH = (atan2(V_2,V_1));%(atan(V_2./V_1));%unwrap(angle(V_1 + V_2*i));
FA = sqrt(HHH.^2+SSS.^2+LLL.^2);
FPHI = acos(FL./FA);


for qa_1 = 1:si(1)
    for qa_2 = 1:si(2)
        if (V_2(qa_1,qa_2) >= 0)
            if (V_1(qa_1,qa_2) >= 0)
                FH(qa_1,qa_2) = ((FH(qa_1,qa_2))./(pi)).^3;
            else
                FH(qa_1,qa_2) = ((FH(qa_1,qa_2))./(pi)).^3;
            end;
        else
            if (V_1(qa_1,qa_2) >= 0)
                FH(qa_1,qa_2) = (abs(FH(qa_1,qa_2))./(pi)).^1;
            else
                FH(qa_1,qa_2) = (abs(FH(qa_1,qa_2))./(pi)).^1;
            end;
        end;
    end;
end;
```

```
w(:,:,1) = FH;
w(:,:,2) = FS;
%w(:,:,3) = FA;
w(:,:,3) = FL;



sz = size(w(:,:,1));
las_x = sz(1) - 2;
las_y = sz(2) - 2;


st_pt_x = 1;
st_pt_y = 1;

for r_s_x = 1:las_x
    for r_s_y = 1:las_y

trt = 1;
[L_1,L_2,L_3] = PH_trinion_typeI_non_localized(w(st_pt_x+r_s_x-
trt:st_pt_x+r_s_x+trt,...
   st_pt_y+r_s_y-trt:st_pt_y+r_s_y+trt,1),w(st_pt_x+r_s_x-
trt:st_pt_x+r_s_x+trt,...
   st_pt_y+r_s_y-trt:st_pt_y+r_s_y+trt,2),w(st_pt_x+r_s_x-
trt:st_pt_x+r_s_x+trt,...
   st_pt_y+r_s_y-trt:st_pt_y+r_s_y+trt,3));

pha = ((atan2(sqrt(L_2.^2+L_3.^2),(L_1))));

for qa_1 = 1:3
    for qa_2 = 1:3
        if (L_1(qa_1,qa_2) >= 0)
            pha(qa_1,qa_2) = ((abs(pha(qa_1,qa_2)))/(pi)).^3;
        else
            pha(qa_1,qa_2) = ((abs(pha(qa_1,qa_2)))/(pi)).^3;
        end;
    end;
end;

 [r_1,r_2,r_3] = Vectorial_PCA_Transform_with_trinions((L_1),(L_2),(L_3));

new_pha = abs(atan2(sqrt(r_2.^2+r_3.^2),(r_1)));

for qa_1 = 1:3
    for qa_2 = 1:3
        if (r_1(qa_1,qa_2) >= 0)
            new_pha(qa_1,qa_2) = ((abs(new_pha(qa_1,qa_2)))/(pi)).^3;
        else
            new_pha(qa_1,qa_2) = ((abs(new_pha(qa_1,qa_2)))/(pi)).^3;
        end;
    end;
end;

new_term =
abs((r_1.^2+r_2.^2+r_3.^2)).*abs(entropy(new_pha./max(new_pha(:))));
Q_Pow_log_scale(r_s_x,r_s_y) = std(std(log(1 + new_term)./log(1 +
max(max(new_term)))));
```

```
term = abs((L_1.^2 + L_2.^2 + L_3.^2).*(abs(sum(sum(pha.^(1/9))))));
TRA(r_s_x,r_s_y) = std(std(log(1 + term)./log(1 + max(max(term)))));

Pow_term = abs((L_1.^2 + L_2.^2 + L_3.^2));
Pow_TRA(r_s_x,r_s_y) = std(std(log(1 + Pow_term)./log(1 +
max(max(Pow_term)))));

clear L_1 L_2 L_3 r_1 r_2 r_3
    end;
end;

toc

figure, imshow(1 - Q_Pow_log_scale./max(abs(Q_Pow_log_scale(:))),[]), box
on
figure, imshow(TRA./max(TRA(:)),[]), box on
figure, imshow(Pow_TRA./max(Pow_TRA(:)),[]), box on
figure, imshow(Pow_TRA,[]), box on
figure, imshow(PCA_Q_Eax./max(PCA_Q_Eax(:)),[]), box on
```

%%%

Max-gradient vectorial technique

```
clear all;

close all;

clc

im=imread('D:\Serki_Test_Images\Output\mri outpu\color31.jpg');

[edge_magnitude, edge_orientation] = coloredges(im);

figure,imshow(im);

title('Original color image');

figure,imshow(edge_magnitude);

title('<Max Garadient based on edge_magnitude>');


figure,imshow(1.0-(edge_magnitude./max(max(edge_magnitude))));

title('Max Garadient based on edge magnitude');
```

```
%%%%%%%%%%%%%%%%%%%%%%%%%%%%%%%%%%%%%%%%%%%%%%%%%%%%%%%%%%%%%%%%%%%%%%%%
%%
```

Classical techniques

```
clear all
close all
clc


I=rgb2gray(imread('C:\Users\serkebme\Desktop\Serki_Test_Images\Output\Class
ical\Matlab_Test_Image\lena.jpg')); %Read in image
IEroberts=edge(I,'roberts'); %Roberts edges
IEprewitt=edge(I,'prewitt'); %Prewitt edges
IEsobel=edge(I,'sobel'); %Sobel edges
IElog=edge(I,'LOG'); %log edges
IEzerocross=edge(I,'zerocross'); %zerocross edges
IEcanny=edge(I,'canny'); %canny edges

subplot(2,3,1), imshow(IEroberts),title('Roberts edge map'); %Display image
subplot(2,3,2), imshow(IEprewitt),title('prewitt edge map');%Display image
subplot(2,3,3), imshow(IEsobel),title('sobel edge map'); %Display image
subplot(2,3,4), imshow(IElog),title('log edge map'); %Display image
subplot(2,3,5), imshow(IEzerocross),title('zerocross edge map'); %Display
image
subplot(2,3,6), imshow(IEcanny),title('canny edge map'); %Display image

figure,imshow(IEcanny,[])
```